



**British
Geological Survey**

NATURAL ENVIRONMENT RESEARCH COUNCIL

Imaging the seabed in shallow water areas (< 300m) using 3D seismic surveys.

Continental Shelf and Margin Programme

Internal Report IR/03/168

Imaging the seabed in shallow water areas (<300m) using 3D seismic surveys.

J. Bulat

editors

A. Stevenson and J.R.Evans.

The National Grid and other Ordnance Survey data are used with the permission of the Controller of Her Majesty's Stationery Office.
Ordnance Survey licence number GD 272191/1999

Key words

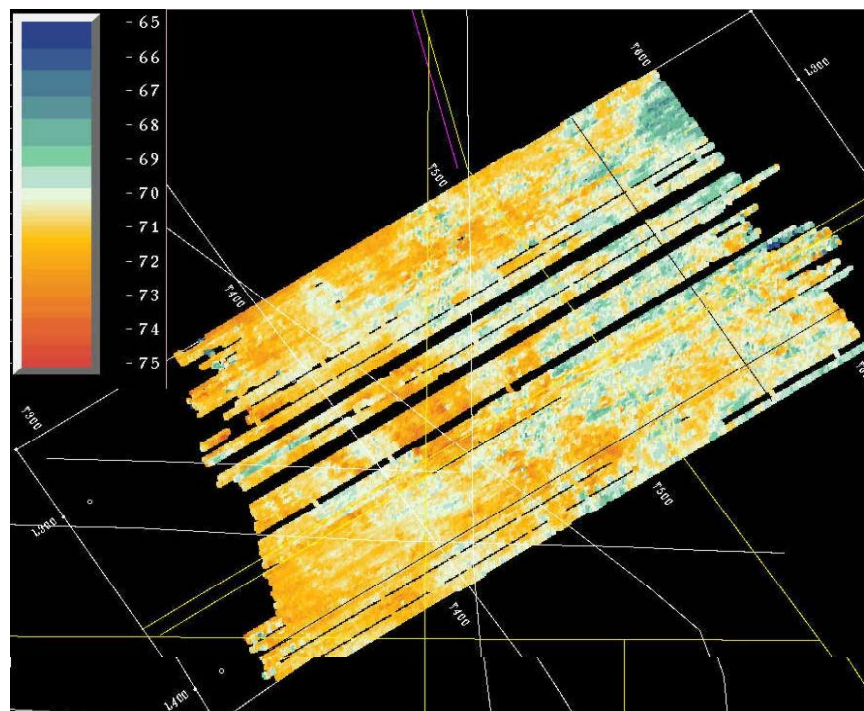
Seabed, Imagery, pre-stack processing.

Front cover

Water depth estimated from auto-correlation pick assuming water velocity of 1480m/s. Scale in metres.

Bibliographical reference

BULAT, J. .2004.Imaging the seabed in shallow (<300m) using 3D surveys. *British Geological Survey Internal Report*, IR/03/168. 28pp.



BRITISH GEOLOGICAL SURVEY

The full range of Survey publications is available from the BGS Sales Desks at Nottingham and Edinburgh; see contact details below or shop online at www.thebgs.co.uk

The London Information Office maintains a reference collection of BGS publications including maps for consultation.

The Survey publishes an annual catalogue of its maps and other publications; this catalogue is available from any of the BGS Sales Desks.

The British Geological Survey carries out the geological survey of Great Britain and Northern Ireland (the latter as an agency service for the government of Northern Ireland), and of the surrounding continental shelf, as well as its basic research projects. It also undertakes programmes of British technical aid in geology in developing countries as arranged by the Department for International Development and other agencies.

The British Geological Survey is a component body of the Natural Environment Research Council.

Keyworth, Nottingham NG12 5GG

☎ 0115-936 3241 Fax 0115-936 3488
e-mail: sales@bgs.ac.uk
www.bgs.ac.uk
Shop online at: www.thebgs.co.uk

Murchison House, West Mains Road, Edinburgh EH9 3LA

☎ 0131-667 1000 Fax 0131-668 2683
e-mail: scotsales@bgs.ac.uk

London Information Office at the Natural History Museum (Earth Galleries), Exhibition Road, South Kensington, London SW7 2DE

☎ 020-7589 4090 Fax 020-7584 8270
☎ 020-7942 5344/45 email: bgs london@bgs.ac.uk

Forde House, Park Five Business Centre, Harrier Way, Sowton, Exeter, Devon EX2 7HU

☎ 01392-445271 Fax 01392-445371

Geological Survey of Northern Ireland, 20 College Gardens, Belfast BT9 6BS

☎ 028-9066 6595 Fax 028-9066 2835

Maclean Building, Crowmarsh Gifford, Wallingford, Oxfordshire OX10 8BB

☎ 01491-838800 Fax 01491-692345

Parent Body

Natural Environment Research Council, Polaris House, North Star Avenue, Swindon, Wiltshire SN2 1EU

☎ 01793-411500 Fax 01793-411501
www.nerc.ac.uk

Contents

Contents.....	i
Summary.....	iv
1 Introduction.....	1
2 Examples of seabed imagery in shallow water (<300m) areas based on conventionally processed 3D seismic.....	2
3 Comparison between swath bathymetry and 3D seismic images.....	5
4 Acquisition and processing design and seabed imagery.....	9
4.1 Constraints in recording the seabed reflection.....	10
4.2 Survey footprint.....	11
5 Indirect estimation of seabed topography from pre-stack data.....	12
5.1 Multiples, auto-correlation & predictive deconvolution.....	12
5.2 Enhancing multiples with CMP processing.....	15
6 Fina 30/14 seismic survey.....	17
6.1 Known seabed geology of the area covered by FINA 30/14 3D survey.....	17
6.2 FINA 30/14 survey geometry and data description.....	20
7 Results of multiple stack processing.....	22
7.1 Near trace section.....	22
7.2 Seabed periodicity pick.....	26
8 Conclusions.....	28
9 Acknowledgements.....	28
10 References.....	29

FIGURES

Figure 1. Seabed shaded-relief image of the Faroe-Shetland Channel. Illumination from NE, bathymetric contours shown in white. Numbered lines and boxes indicate position of text figures presented in this report.	1
Figure 2. Profile across 3D survey woc96, location shown on figure 1. Note how the seabed reflection suddenly fades at 400ms (c. 300m) and becomes progressively contaminated with noise as the seabed shallows.	2
Figure 3. Plot of seabed amplitude (Y-axis) vs two-way time (X-axis) for the woc96 survey. Reproduced from Bulat (2003).	3
Figure 4. Shaded relief image over the Clair field. Illumination from the NW	3
Figure 5. Detailed shaded relief image of the 'Vrackie' dataset. Illuminated from NE. Arbitrary profile AA' also shown. Note the increasing noise at depths shallower than 300m.	4
Figure 6. Shaded relief image of the seabed pick derived from 3D seismic data (30m by 25m grid) illuminated from the northeast. The swath outline and 100m depth contours are superimposed in white. Profile locations AA' to DD' are shown in red and displayed in Figure 9.	5
Figure 7. Shaded relief image of the BP swath bathymetry with 100m bathymetric contours and interpretations are superimposed.	6
Figure 8. Difference map between 3D seismic survey and BP swath bathymetry with 100m bathymetric contours superimposed. The map is colour coded for a range of +15m to -15m.	6
Figure 9. Comparison of depths between swath and 3D seismic along profiles AA' to DD'. Swath depths are drawn in black, 3D pick depths in grey. Location of profiles are shown on Figure 6	8
Figure 10. Schematic diagram illustrating relationship between water depth, seabed velocity and offset in determining the refraction event arrival distance along a hydrophone in typical 2D-acquisition geometry.	10
Figure 11. Ray paths of common multiple classes. After Hatton et al. (1986)	13
Figure 12. Use of auto-correlation to recognise periodicity in time series data in the presence of noise. After Hatton et al. (1986).	14
Figure 13. The auto-correlation of a random time series, after Hatton et al. (1986). Left panel, random time series, right panel its auto-correlation.	14
Figure 14. Example CMP displays from the Fina 30/14 survey. Top Panel; raw CMP gather, showing refraction and seabed reflection events and their apparent velocities. Bottom Panel; same CMP gather after the application of NMO with single velocity of 1500 m/s.	16
Figure 15. Study area showing BGS line tracks, BGS sample sites (pink circles) and outline of 3D seismic survey (red line) FINA 30/14 used in this study.	17
Figure 16 .Pinger profile BGS 76/4-9. Fixes 2-6 showing variation in thickness of Forth Formation. Time lines 10ms.	18
Figure 17. Regional bathymetry contours from 1:250K digbath compilation. BGS profiles shown in black. UK block boundaries and median line shown in red.	19
Figure 18. Shot location map	21
Figure 19 . CMP fold coverage	21

Figure 20 . Example line 397 of near-trace volume with no mutes applied. The yellow horizon is the primary seabed reflection, the cyan is the first seabed multiple and the green horizon is the seabed pick derived from an auto-correlation volume. 22

Figure 21. Example trace display (trace 452). Note the poor continuity and the abrupt changes of level of the seabed event. Note also the overall drop in amplitude between Lines 320-330 and 383-415, which are artefacts of the survey design..... 23

Figure 22. Map view of two-way time Zap of the seabed reflection. Note the strong impact of survey footprint artefacts and abrupt changes of levels between swaths. 24

Figure 23. Map view of amplitude of seabed reflection event. Amplitudes also show strong footprint artefacts and changes between swaths..... 24

Figure 24. Map view of seabed multiple horizon. Note the reduced footprint and swath to swath shifts, so that structures are clearer. Note also the cycle skip artefacts in the south. 25

Figure 25. Amplitude map of the first seabed multiple horizon. Note the appearance of more trends in comparison to the amplitude map for the primary reflection. 25

Figure 26 . Example Line 387 from the auto-correlation volume designed around the first multiple 26

Figure 27 . Water depth estimated from auto-correlation pick assuming water velocity of 1480m/s. Scale in meters. 27

Figure 28. Amplitude map of seabed pick based on an auto-correlation volume. Scale in arbitrary units. 27

TABLES

Table 1. Statistics for difference map within different bathymetric ranges. All values are in metres..... 7

Table 2. Basic parameters of the FINA 30/14 3D seismic survey. 20

Summary

This report discusses imaging the seabed from exploration 3D seismic data in shallow water areas, defined as less than 300m. The issues involved are discussed primarily with reference to data sets within the Faroe-Shetland Channel (FSC) where the bulk of the seabed imaging work has been performed and where the availability of other data such as swath bathymetry permit detailed comparison.

The report then considers how seafloor conditions and survey design influence seabed reflection quality. A method for mapping seabed topography using seabed multiple energy is presented and applied to the FINA 30/14 3D survey in the Central Graben of the North Sea.

The major conclusions of this report are:

- (1) In water depths shallower than 300-400m and in areas of high seabed velocity, the seabed reflection on conventionally processed 3D seismic volumes tends to become poorly imaged if the survey has been designed for deep targets.
- (2) Pre-stack processing of the seismic volume to enhance seabed multiples does appear to generate a plausible surface on the Fina survey. The first multiple is less contaminated with survey footprint artefacts than the primary reflection. The auto-correlation pick provides the most coherent surface in this study. An unresolved question is the extent to which the derived topography reflects tuning effects due to the rapidly varying thickness of the Forth Formation, as opposed to the true seabed topography.
- (3) The technique may usefully be applied to another, deeper water area, such as Shell's woc96 survey in the FSC where the primary seabed reflection begins to fade. This would enable a direct comparison of surfaces generated by conventional and multiple enhancement processing as well as present an opportunity to extend the FSC seabed image.

1 Introduction

Seabed imagery in the Faroe-Shetland Channel (FSC), based on picking the seabed on 3D seismic data has been particularly valuable in helping to understand processes forming the seabed (Bulat and Long, 2001; Long, Bulat & Stoker, in press). Figure 1 is the current version of the seabed image in the FSC. In deep water areas the image quality is excellent. However, in water depths shallower than 300m the results have been mixed. This report will discuss the issues posed in imaging the seabed in shallower waters, a quantitative comparison with swath bathymetry, a discussion of the likely causes of poor imaging and propose an indirect methodology based on seabed multiples that may be able to image the seafloor in shallow water.

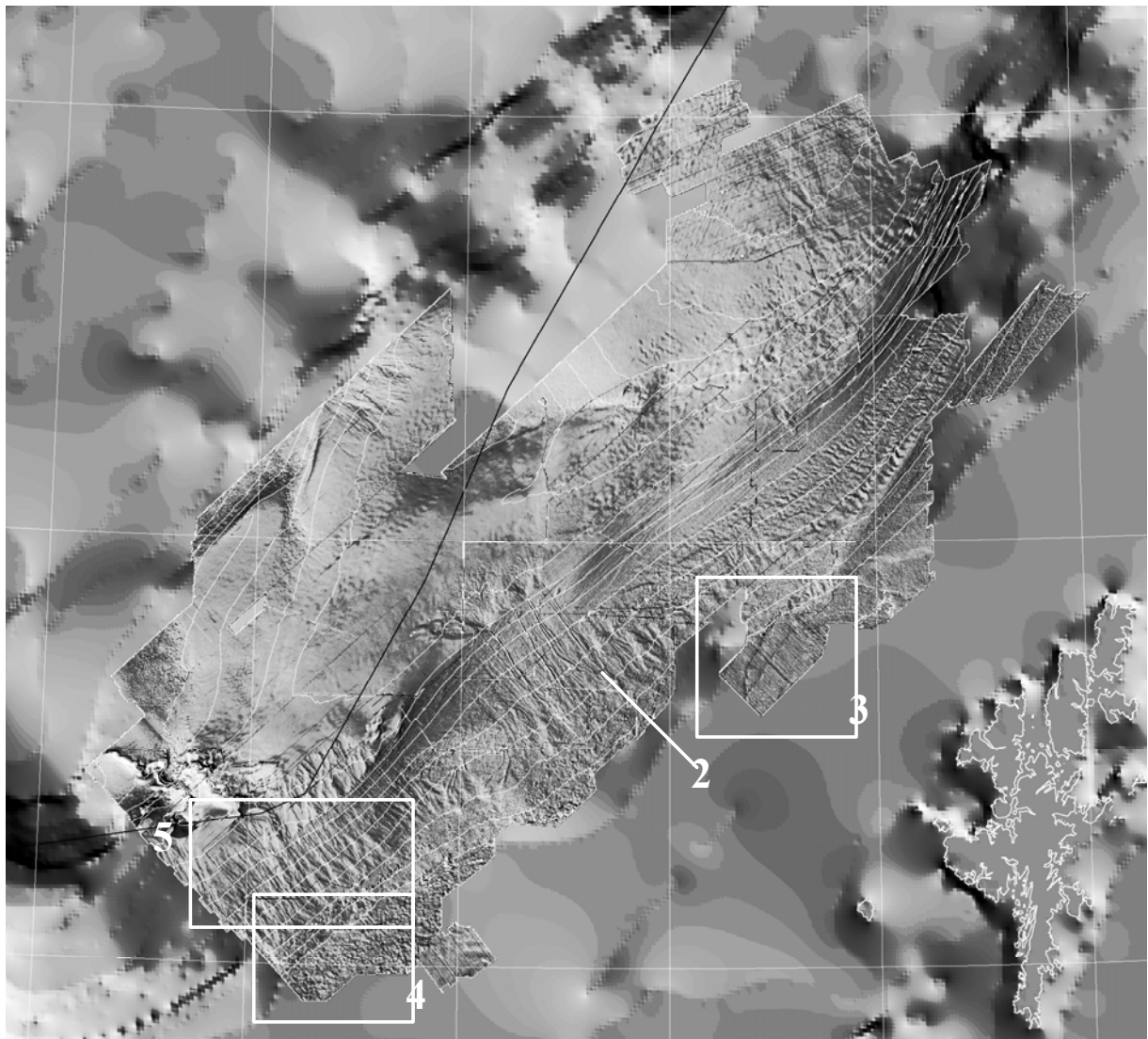


Figure 1. Seabed shaded-relief image of the Faroe-Shetland Channel. Illumination from NE, bathymetric contours shown in white. Numbered lines and boxes indicate position of text figures presented in this report.

2 Examples of seabed imagery in shallow water (<300m) areas based on conventionally processed 3D seismic.

The seabed image for the Faroe-Shetland Channel covers a large bathymetric range of 200m to 1700m. The image quality in the shallow water areas of the West Shetland Shelf is of variable quality. Some datasets show excellent detail in water depths of 200m, whereas others exhibit very weak events often partially masked by coherent noise at similar or greater depths. Figure 2 shows a profile across the Shell woc96 dataset where the seabed event becomes increasingly contaminated with noise such that the seabed pick was terminated at 400ms two-way time. Note the sudden drop in amplitude and the increasing strength of the survey footprint artefacts, seen as pronounced two-way time displacements from line to line. Figure 3 shows a plot of amplitude against two-way time for the woc96 dataset demonstrating a pronounced linear relationship that is probably an artefact of incorrect amplitude compensation for the reduction in effective fold due to refraction energy muting. Figure 4 shows the seabed image over the Clair field generated from seabed picks provided by BP. The Clair image shows convincing morphology that testifies to the presence of minor moraine ridges as well as major terminal moraines marking the major glaciations known in this area.

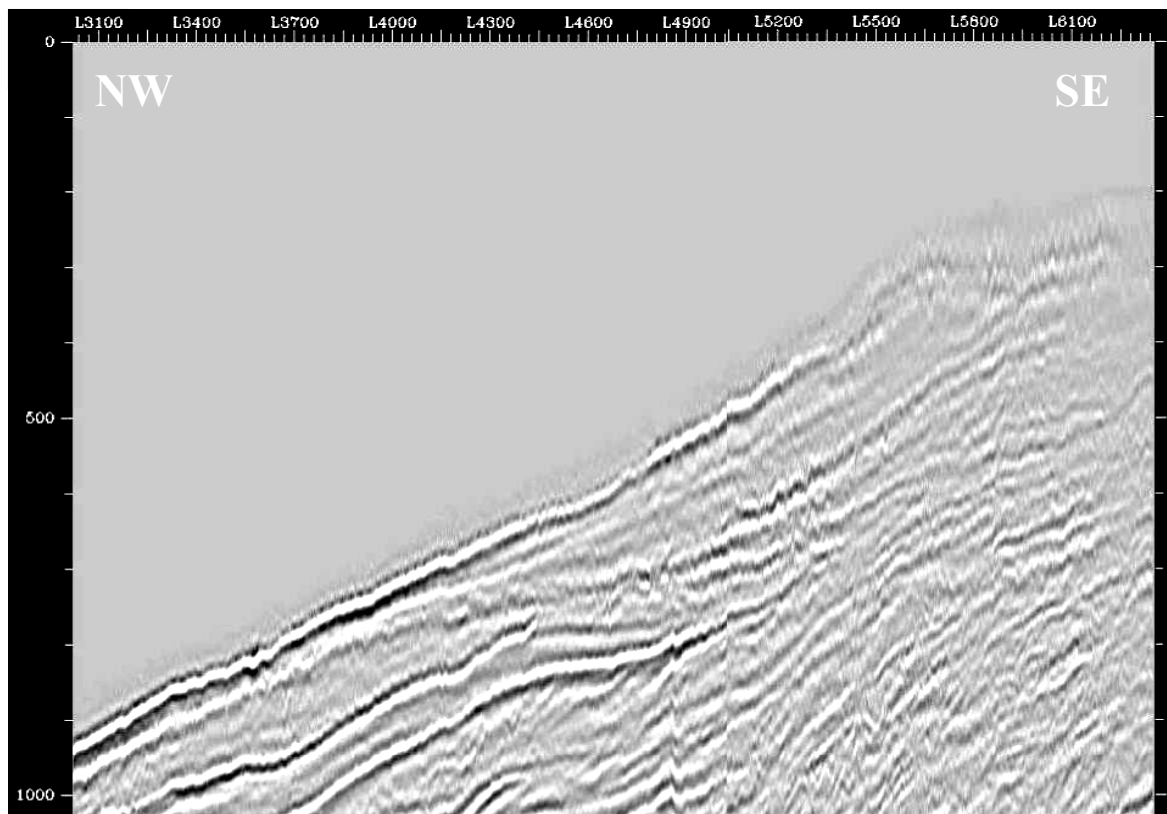


Figure 2. Profile across 3D survey woc96, location shown on figure 1. Note how the seabed reflection suddenly fades at 400ms (c. 300m) and becomes progressively contaminated with noise as the seabed shallows.

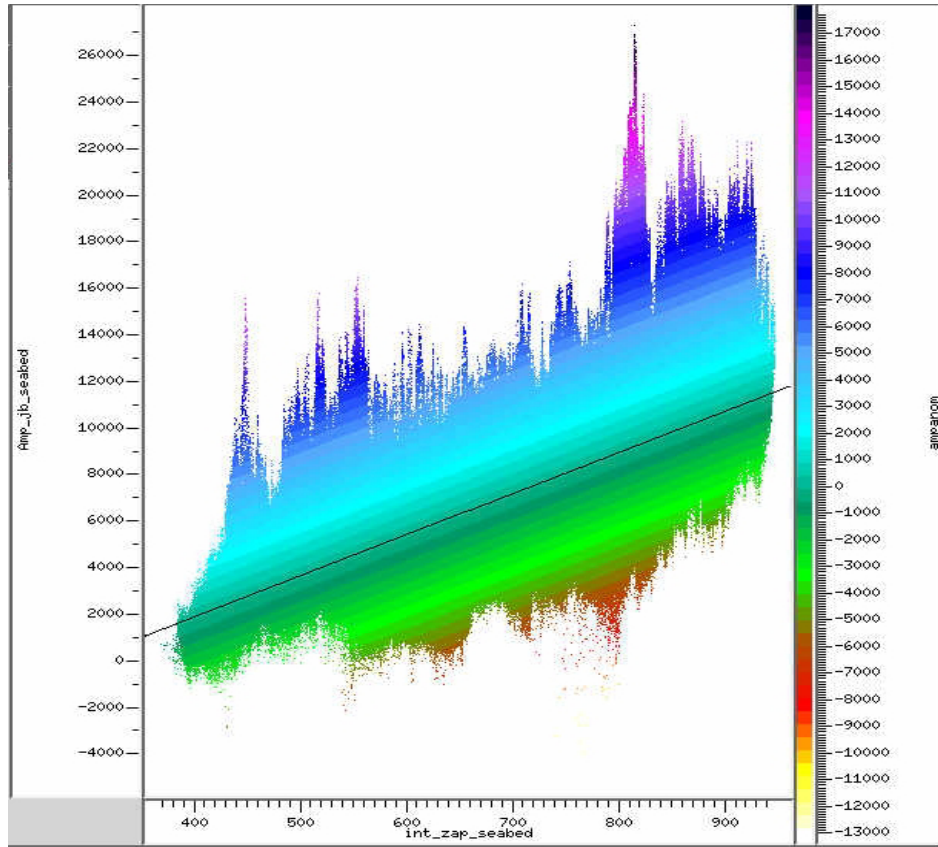


Figure 3. Plot of seabed amplitude (Y-axis) vs two-way time (X-axis) for the woc96 survey. Reproduced from Bulat (2003). The colour bar represents the deviation of the observed amplitude value from the linear least squares trend calculated for the distribution.

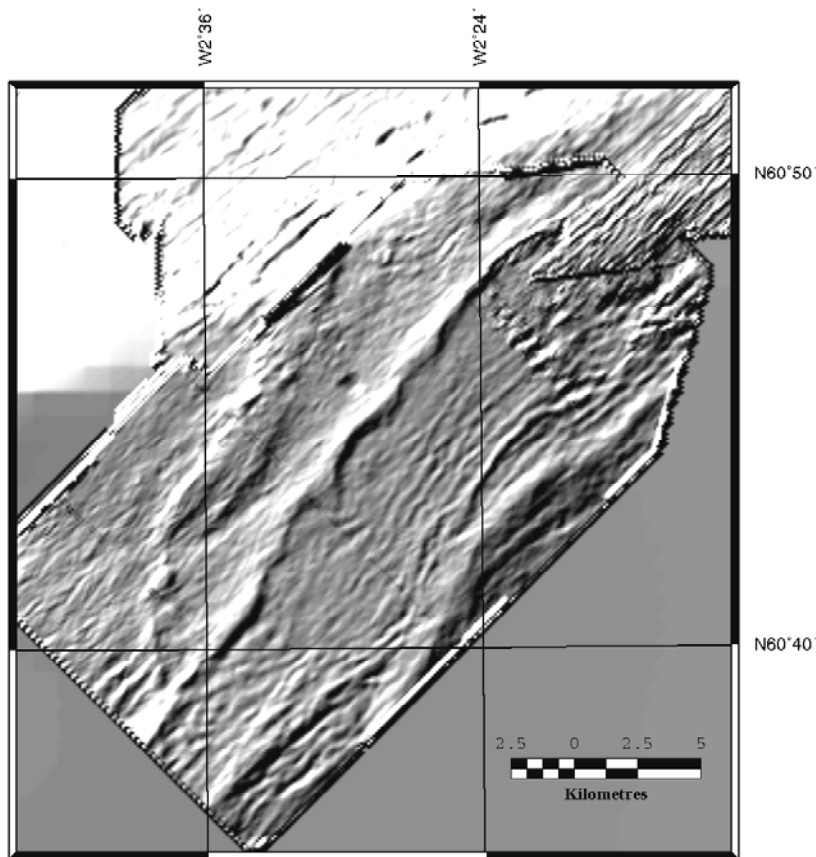


Figure 4. Shaded relief image over the Clair field. Illumination from the NW

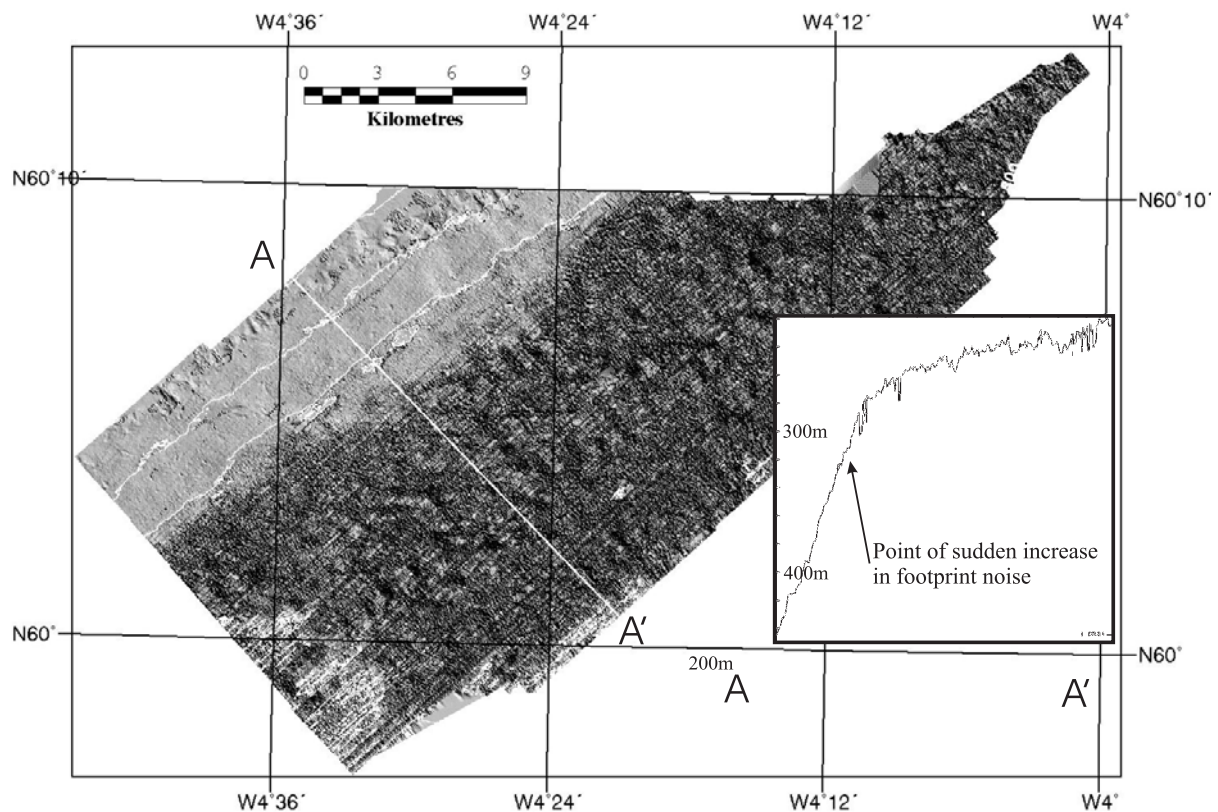


Figure 5. Detailed shaded relief image of the 'Vrackie' dataset. Illuminated from NE. Arbitrary profile AA' also shown. Note the increasing noise at depths shallower than 300m.

The sediments over Clair are known to be over-compacted (and therefore of higher velocity than the soft sediments found on the slope) in approximately 200m of water. In contrast, the Vrackie dataset in the south-eastern part of the FSC image and displayed as Figure 5, shows pronounced survey footprint artefacts that give rise to a very irregular surface at water depths less than 300m (400ms). This is consistent with the picture obtained from the woc96 dataset shown in Figure 2. Furthermore, high-resolution BGS profiles over the same area show that the seabed is not as rough as this image suggests (Bulat & Long, 2001), which lends credence to the interpretation of the irregular topography as being an artefact. Figure 4 also shows that the onset of the irregular topography is not wholly a function of two-way time in that it does not slavishly follow the bathymetric contour.

3 Comparison between swath bathymetry and 3D seismic images.

A more quantitative assessment of the quality of 3D seismic imagery can be obtained by comparison with swath datasets. In the Schiehallion, Foinavon area, BP commissioned an extensive swath bathymetry survey, which has provided a unique opportunity to make a detailed comparative study. Figure 6 shows the shaded relief image of the seabed pick derived from 3D seismic surveys and Figure 7 shows the shaded relief image of the swath grid. Figure 8 is a difference grid between these two data sets that has been colour coded to represent the data range. Table 1 demonstrates that the differences between 3D seismic and swath bathymetry in deep water areas (>500m) are small. Inspection of Figure 8 confirms that this region shows relatively gentle, long period changes, predominantly associated with survey footprint. For intermediate depths (400-500m) the difference map shows up shorter period features, mostly due to misalignment of topography (see profile C inset on Figure 9). The mean and median differences are significantly increased. For shallow water areas (<400m) the mean and median differences are highest and the map shows many short period features that are due to increasing noise levels on the 3D seismic pick as well as the misalignment of features.

Profiles A-C show close agreement in the short wavelengths. The differences are in the very long wavelengths and can be attributed to more precise water velocity measurements on the swath data. The detail inset panel on profile C shows that there is evidence for a lateral displacement between the two surveys of up to 142m. This may be due to errors in migration parameters or navigational errors. Profile D shows the least agreement between the two data sets. This is attributed to increased noise on the 3D pick in shallower water depths.

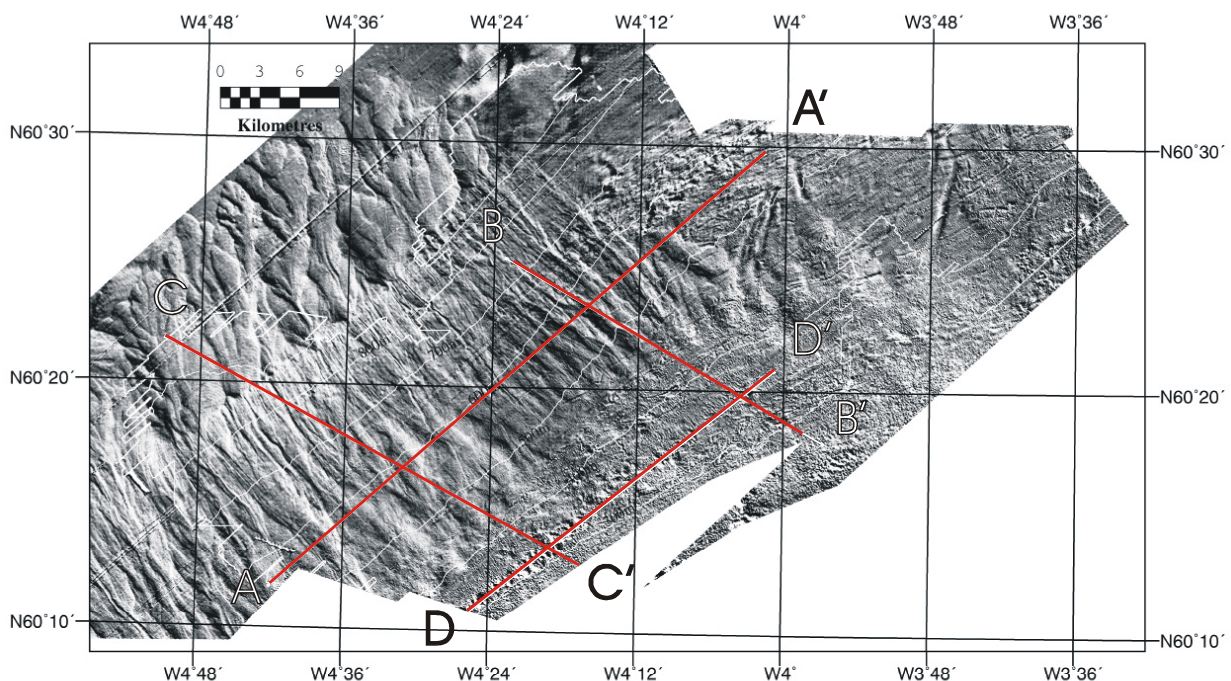


Figure 6. Shaded relief image of the seabed pick derived from 3D seismic data (30m by 25m grid) illuminated from the northeast. The swath outline and 100m depth contours are superimposed in white. Profile locations AA' to DD' are shown in red and displayed in Figure 9.

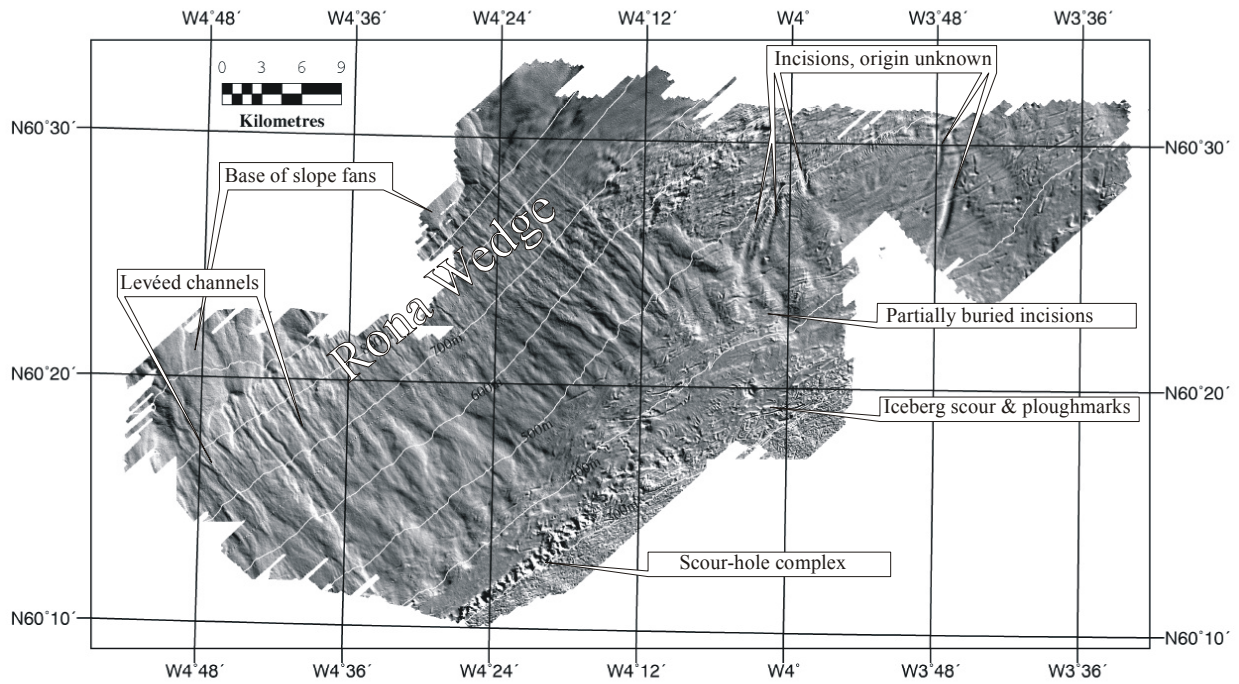


Figure 7. Shaded relief image of the BP swath bathymetry with 100m bathymetric contours and interpretations superimposed.

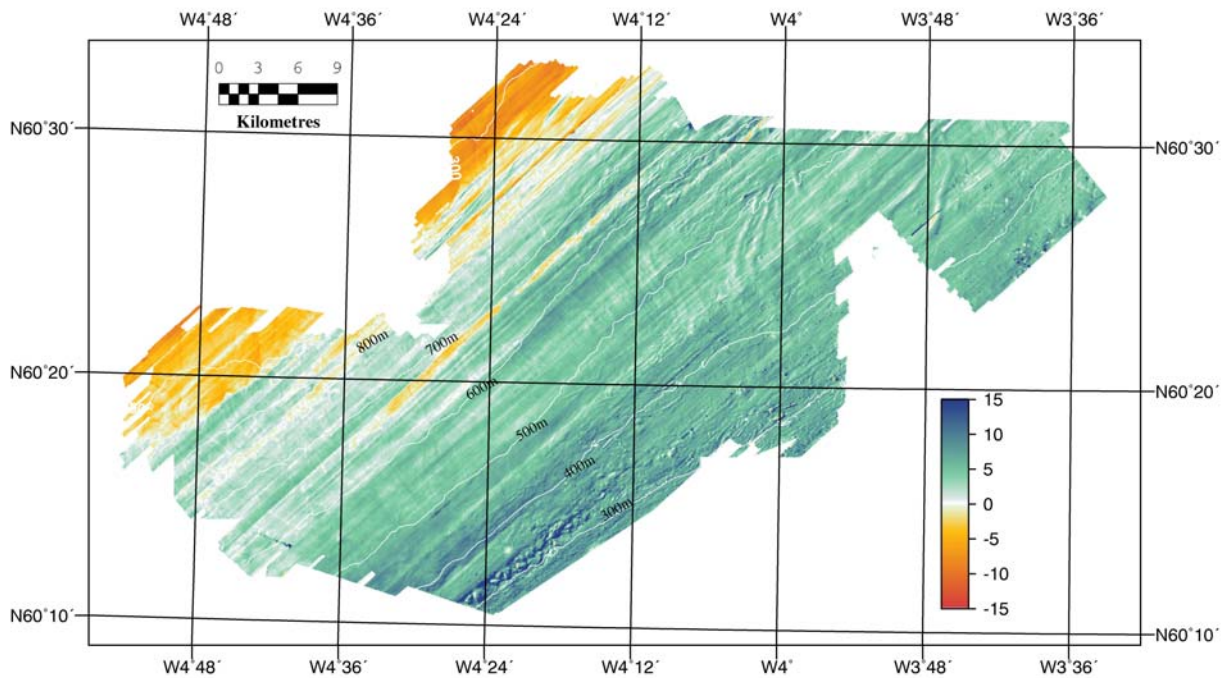


Figure 8. Difference map between 3D seismic survey and BP swath bathymetry with 100m bathymetric contours superimposed. The map is colour coded for a range of +15m to -15m.

	<400m	400-500m	>500m	All
MIN	-6.924	-3.994	-17.312	-17.312
MAX	33.372	23.881	27.701	34.182
MEAN	6.188	4.698	1.274	3.034
MEDIAN	5.826	4.608	1.854	3.608

Table 1. Statistics for difference map within different bathymetric ranges. All values are in metres.

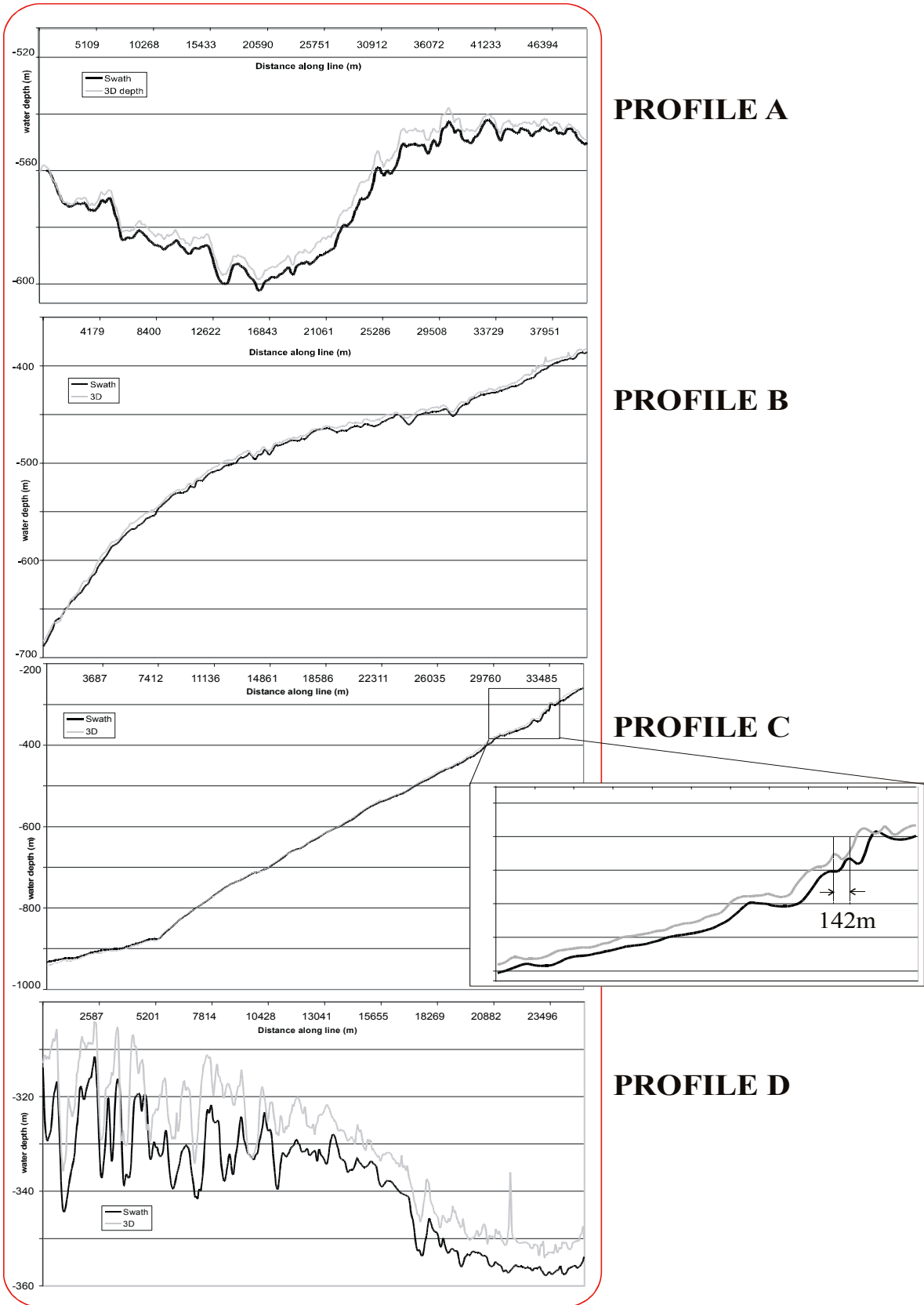


Figure 9. Comparison of depths between swath and 3D seismic along profiles AA' to DD'. Swath depths are drawn in black, 3D pick depths in grey. Location of profiles are shown on Figure 6.

4 Acquisition and processing design and seabed imagery.

A full description of 2D and 3D seismic acquisition and processing is presented in Yilmaz (2001). What follows is a brief review of some basic concepts pertinent to seabed imagery. In many ways 3D seismic acquisition is simply an extension of 2D multi-channel profiling, where a receiver cable composed of many individual hydrophone groups is towed behind an acoustic source. The response of each group to an individual shot is digitally recorded as a separate data channel, which is associated with a particular offset distance i.e. the distance from the source to the centre of the individual hydrophone group. The result of this procedure is a shot record or gather composed of many channels. The length of cable and number of hydrophone groups used in any particular survey are determined by the target depth. Cable lengths of many kilometres are common, resulting in hundreds of channels in a shot gather.

Acoustic noise, both random and coherent, is always present in seismic data, masking those events associated with geological structure. The advantage of multi-channel data is that it provides large-scale data redundancy, so that statistical techniques can be used to reduce noise levels considerably. Central to this procedure is the idea of the Common Mid Point (CMP), a.k.a. Common Depth Point (CDP). In principle, this is an extension of the idea of the vertical stack in land seismic acquisition, where shots are repeated with the same shot and receiver locations and the resultant traces added together. This simple statistical procedure attenuates random noise, whereas coherent energies are added or stacked.

In the marine environment it is not feasible to stop a ship and repeatedly record many traces for the same shot and receiver locations. So other means are used to achieve the same objective from data that is continuously acquired. If it is assumed that reflections come from flat horizontal reflectors in the subsurface, then a CMP can be defined that lies halfway between the source and hydrophone group. Furthermore, by firing the sources at exact multiples of the group distance, a set of traces will exist, coming from many shot gathers, that are associated with any one CMP. Thus CMP gathers can be assembled from continuously acquired shot gathers. Each trace within the CMP gather has a different offset and has taken a different ray path to the CMP. Because of the differing ray paths, the arrival times increase with offset, a behaviour termed normal move-out (NMO). It can be shown that reflections and multiples exhibit a hyperbolic form when displayed as a time-offset panel. The curvature of the hyperbola is a function of the mean velocity above the reflector. Low velocities are seen as steep sided hyperbolae; high velocities are observed as shallow sided hyperbolae. The NMO can be corrected for by stretching the CMP gather so that primary events line up. The stretch is a function of the average velocity, and involves an interpretation procedure known as velocity analysis, where a geophysicist, in effect, decides which events are primary reflections, by picking a suitable velocity-time function. Once the stretch is applied, the traces in the CMP gather may be summed i.e. stacked, a procedure which reinforces coherent reflections to a greater degree than noise. When properly applied, this is a powerful technique for attenuating random noise in the section.

3D seismic acquisition differs from the 2D case in that many cables and sources are towed simultaneously with fixed lateral displacements, thus giving a kind of swath coverage rather than a simple profile. As sources and hydrophone groups are no longer in-line, instead of CMP locations along lines, CMP bins are defined where a trace within any CMP bin has an azimuth angle relative to the line direction associated with the source-receiver pair, as well as offset distance. Similarly, the velocity analysis is three dimensional, where the 2D hyperbola becomes a 3D hyperbolic surface.

4.1 CONSTRAINTS IN RECORDING THE SEABED REFLECTION.

3D seismic surveys are designed to optimally image specific exploration targets. Deep targets require larger sources and longer hydrophone cables to record greater offset distances. Shallow targets need shorter cables and smaller offset distances as well as shorter minimum offset between source and cable. A general rule of thumb is that the offset range should equal the target depth, as this gives the most accurate velocity analysis over the target.

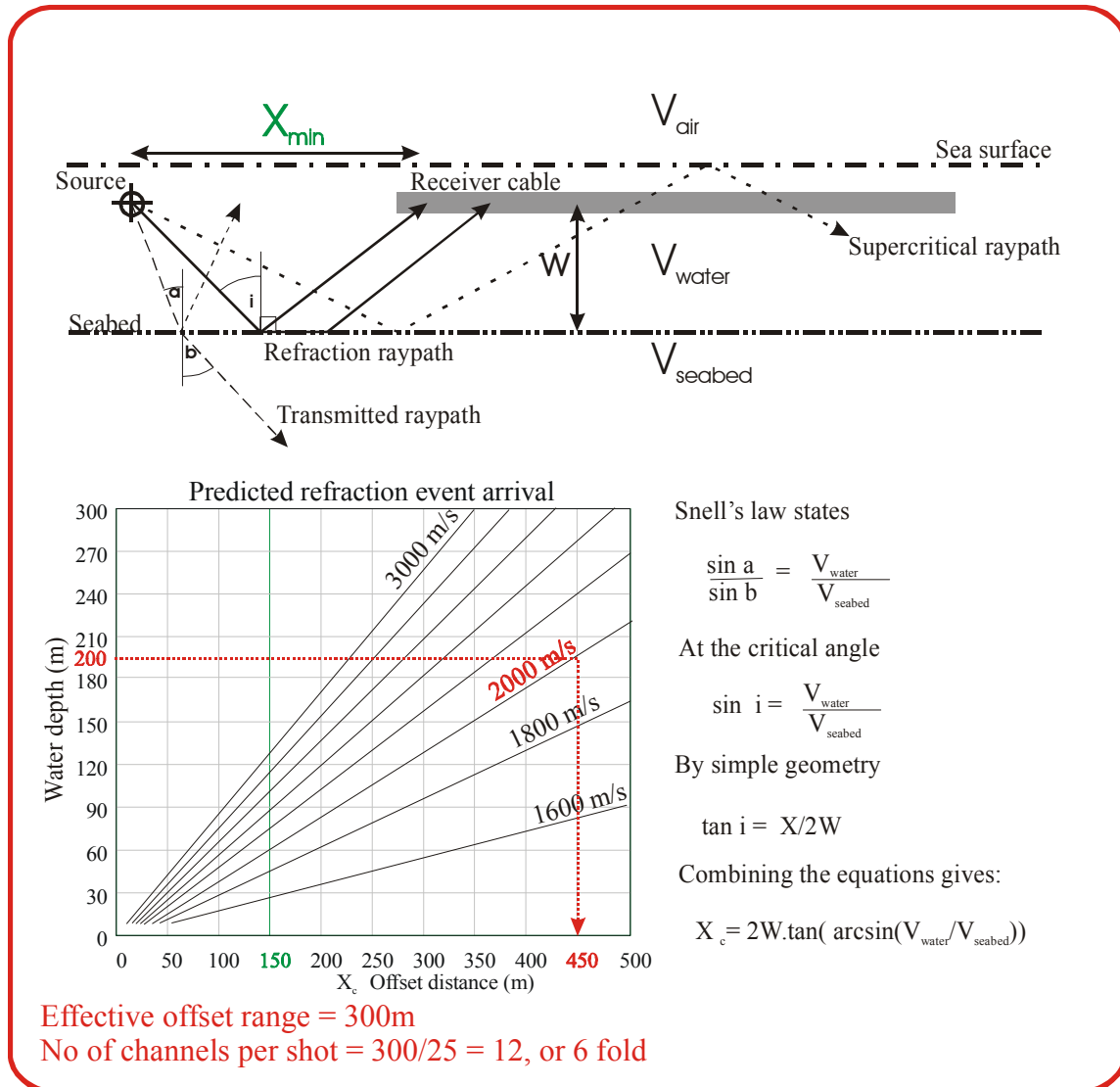


Figure 10. Schematic diagram illustrating the relationship between water depth, seabed velocity and offset in determining the refraction event arrival distance along a hydrophone string in a typical 2D-acquisition geometry.

The minimum offset distance for commercial 2D and 3D seismic surveys is often in the region of 100-150m. Such distances are required to reduce the impact of noise generated by the passage of the ship and airgun arrays through the water. The propagation of sound exhibits the same phenomena as found in optics. Thus in addition to direct reflections, other events such as refraction and total internal reflection, as determined by Snell’s law, are commonly observed on seismic records. Figure 10 shows the typical geometry of a 2D-acquisition system and displays a graph showing the refraction arrival distance X for a range of water depths and seabed velocities. Beyond this distance the records will be dominated by the total internal reflection energy (a.k.a. supercritical energy) generated at the sea-air and sea-bed interfaces. The distance X therefore

represents the maximum offset at which a seabed reflector can be recorded before being masked by refractions or supercritical energy. With a minimum offset of 100m it is clear that in very shallow water and hard bottom conditions the seabed reflection may not be recorded at all, or may appear only within a very small offset range. Thus a recognisable seabed return is observed on only a few traces resulting in a very weak signal after stacking. In the FSC, glacial sediments, particularly over-compacted diamictos, dominate the shallow water shelf margin. Stoker (1999) calculated from reconciling BGS shallow boreholes and BGS seismic, that the seismic velocities of the near surface sediments on the slope varied from 1.5 km/s to 1.6 km/s. The seabed on the slope is generally covered by normally – to under-consolidated muddy sediments (Paul et al., 1993). In contrast, the shelf sediments have velocities between 1.8 km/s to 2.0 km/s, due to these sediments being predominantly over-compacted glacial diamictos. A sharp drop of seabed velocity at the shelf break, may explain the sudden change in the level of survey footprint noise at this point on Figure 5.

Regrettably, the acquisition and processing reports for these surveys have not been provided to us, so it is impossible to confirm that the difference in image quality observed on the surveys is due, as we suspect, to very different acquisition geometries. However, as the Clair survey was certainly intended to image the relatively shallow Clair field at 2km depth (Coney et al., 1993), it is highly likely that the survey design would sample the close offsets.

4.2 SURVEY FOOTPRINT

Close examination of the seabed image of the FSC reveals the presence of minor time shifts between lines giving rise to a corrugated effect (Bulat and Long, 2001). These features correlate with acquisition direction and are interpreted as systematic noise. Although present throughout the image they become progressively more severe in shallower waters, as demonstrated in Figure 5. Marfurt et al. (1998) define such acquisition related noise as survey footprint and point out that it affects both phase and amplitude. Examination of seabed reflection strength confirms that the systematic noise identified on the seabed image correlates with strong line-to-line amplitude variation (Bulat 2003). There is no one single cause. The literature presents the following causes for marine data:

4.2.1 Feathering

A typical 3D marine survey involves towing multiple receiver streamers and one or more airgun arrays. This basic design should result in a swath of CMP bins where each bin has the same number of traces, i.e. the same fold. These traces will have similar offsets, azimuths and are spatially located at the centre of the bin. However, maintaining such a survey configuration in the presence of strong crosscurrents is very difficult. Streamers start to feather, i.e. the hydrophone is progressively displaced laterally such that the tail of the hydrophone cable is significantly off-line. The resultant CMP distribution becomes rather complex. Firstly, instead of a uniform fold for each bin, a pattern of variable fold is produced. This also implies that the offset and azimuth range for each bin varies. Secondly, the traces are not located at the centre of the bin, but will be systematically scattered. This has a number of knock-on effects. Firstly, it degrades the velocity analyses. As the traces are no longer from exactly the same subsurface location, they no longer exhibit a truly hyperbolic NMO. Once stacked with these subtly incorrect velocities the resultant stack volume will display modulated amplitudes and frequency loss due to misalignment of the events. Hill et al. (1999) performed a simple modelling study to examine variation in footprint due to small errors in velocity analyses on the stacking process. They found that significant footprint patterns were generated with slight velocity errors and that these patterns changed with time, so precluding correction with a simple amplitude scaling function. In marine data, feathering appears to be the main source of acquisition footprint.

4.2.2 Poor acquisition design

Lansley (1996) points out that the optimum 3D survey would have offset and azimuth distributions within CMP bins that were spatially consistent and of high fold. However, in practice uniform sampling is difficult to achieve, and the lack of uniformity results in a pattern of data acquisition lineations. Most conventional 3D surveys have swaths in rectangular patterns, rarely more than 250m wide and many (3-6) kilometres long. If there is insufficient overlap between such swaths, then CMP bins on the edge may be populated with fewer traces than at the centre of the swath. Furthermore, these traces may be associated with a limited range of source-receiver azimuths. The lack of uniformity in fold and azimuth can result in footprint anomalies.

4.2.3 Processing errors

The impact of footprint artefacts is likely to be greater at smaller two-way times, where the errors in static corrections are likely to be greatest, giving rise to errors in velocities. A major uncertainty is likely to be cable depth. In processing, it is typically assumed that the cable is at a constant depth below sea level. Usually, this is achieved by using the drag of the cables through the water to maintain the cables under tension. However, there is also the need to maintain a sufficiently low speed over the subsurface so that the firing interval is maintained in distance and a suitable time window is available to record. These two requirements can conflict in certain oceanographic states, such as following seas. Consider a survey specification which requires that the shot interval should be 25m and 10s record length is required. If the ship travels over the subsurface at 4 knots, approximately 2m/s, then the time required to travel 25m is 14.5s. This provides ample time to record 10s of data and sufficient drag in the water to maintain cable depth. However, in a following sea of say 3 knots, then the ship will need to reduce its speed relative to the water to 1 knot, resulting in low cable tension giving rise to ‘snaking’ of the cable both vertically and horizontally. Small time shifts of this sort are more significant for the smaller arrival time of the primary seabed reflection, than for the multiples.

5 Indirect estimation of seabed topography from pre-stack data.

Where seabed conditions and survey geometry conspire to make the primary seabed reflection weak and contaminated with footprint artefacts, indirect means may be used. Thus study will focus on using seabed multiple energy to estimate seabed topography.

5.1 MULTIPLES, AUTO-CORRELATION & PREDICTIVE DECONVOLUTION

The aim of conventional processing is to reduce the observed seismic response measured as time series at receiver locations to a data set that reveals the underlying acoustic impedance contrasts generated by geology. A very important aspect of this process is the suppression of multiples.

As a seismic wave propagates through layered media, part of the energy of the wave is refracted and part transmitted at each interface according to Snell’s law. This occurs for upward ray paths as well as downward ray paths. Thus the primary reflection is only one among many possible ray paths reverberating between source and receiver. These other ray paths are called multiples because they involve multiple reflection between several interfaces. Figure 11 is a schematic diagram (after Hatton et al., 1986) showing the various classes of multiples. Because the greatest velocity and density contrasts occur between the air-water and water-seabed interfaces, the multiples associated with these interfaces are by far the strongest. Many techniques have been developed to suppress multiples. However, in the context of this study, they may also provide an

indirect means for imaging the seabed. Predictive deconvolution is a commonly used technique to suppress multiples in shallow water areas. This is a filter that attenuates features that repeat with a certain periodicity, termed the prediction lag. Estimating the time lag from noisy time series data can be difficult. However, a statistical technique, called auto-correlation, exists that recognises the periodicity in the presence of noise.

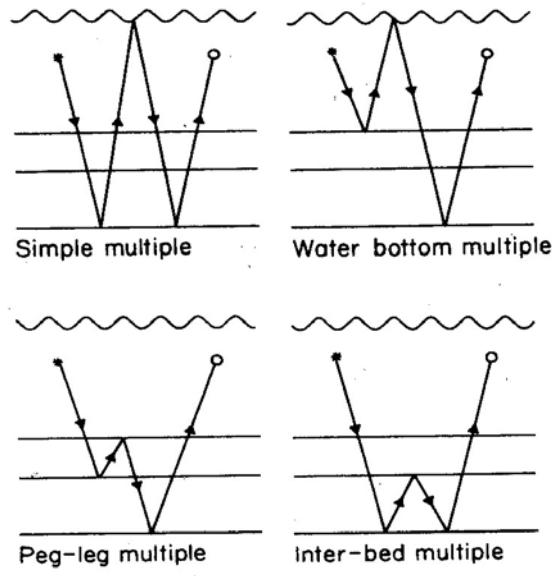


Figure 11. Ray paths of common multiple classes. After Hatton et al. (1986)

A full description of the auto-correlation function is presented in Hatton et al. (1986). Auto-correlation is commonly used to recognise periodicity in noisy time-series data. Figure 12 shows a periodic function, representing a series of multiples, with and without noise, and the calculated auto-correlation functions. As can be seen, even with severe noise added, the auto-correlation is very robust and reveals the major periodicity. Ordinarily, this allows the processor to design an appropriate deconvolution filter to collapse the multiple train into the primary. In comparison, the auto-correlation of a random time series gives values an order of magnitude lower, as is seen in Figure 13. Auto-correlation and predictive deconvolution are widely used in seismic processing. However, in order to work, there has to be a statistically significant number of multiples in the section. In deeper water, this may be problematic. If only 5s of data, say, is recorded, and water depths are 100ms, then there are up to 50 possible seabed multiples in the data volume. If water depths are at 1000ms two-way time then there are only 5 possible seabed multiples present. In the latter case, the small number of multiples may cause predictive deconvolution to fail.

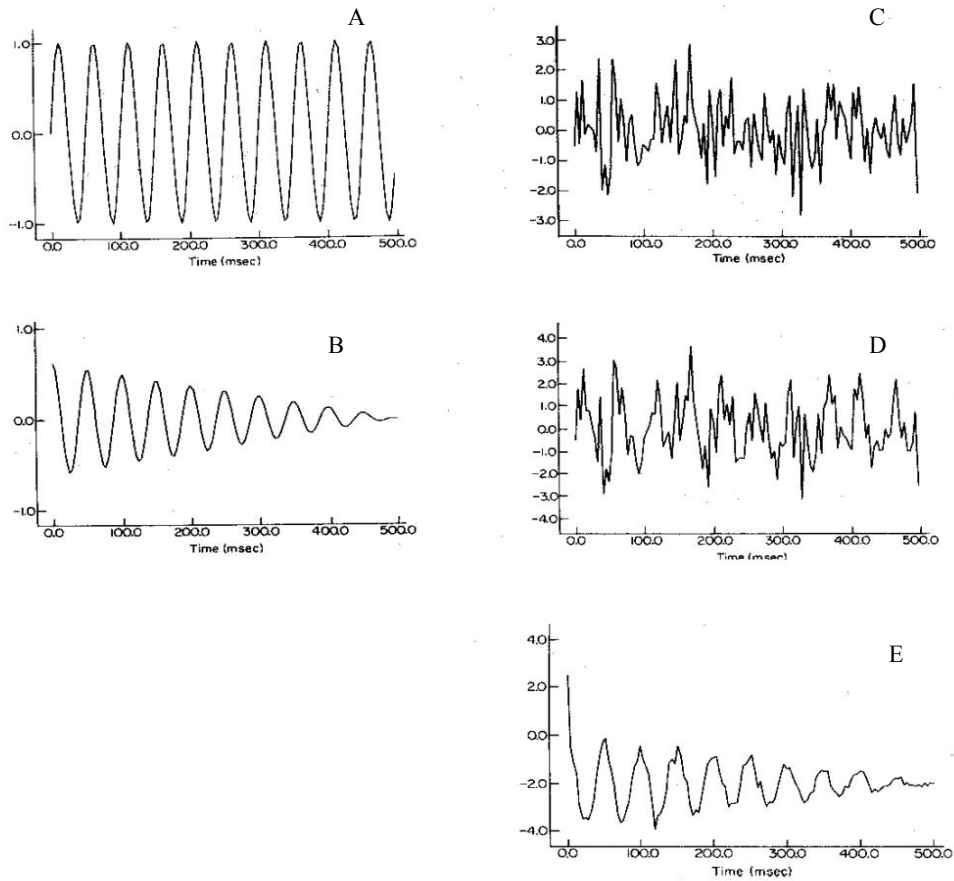


Figure 12. Use of auto-correlation to recognise periodicity in time series data in the presence of noise. After Hatton et al. (1986).

Panel A; A sinusoid of 20Hz. Panel B; The auto-correlation of the sinusoid in A. Panel C; pure noise with Gaussian distribution of zero and unit variance. Panel D. Summation of A & C. Panel E; the auto-correlation of D. Note that the periodicity in the time series D is difficult to perceive because of the noise, whereas the auto-correlation function E reveals its presence clearly.

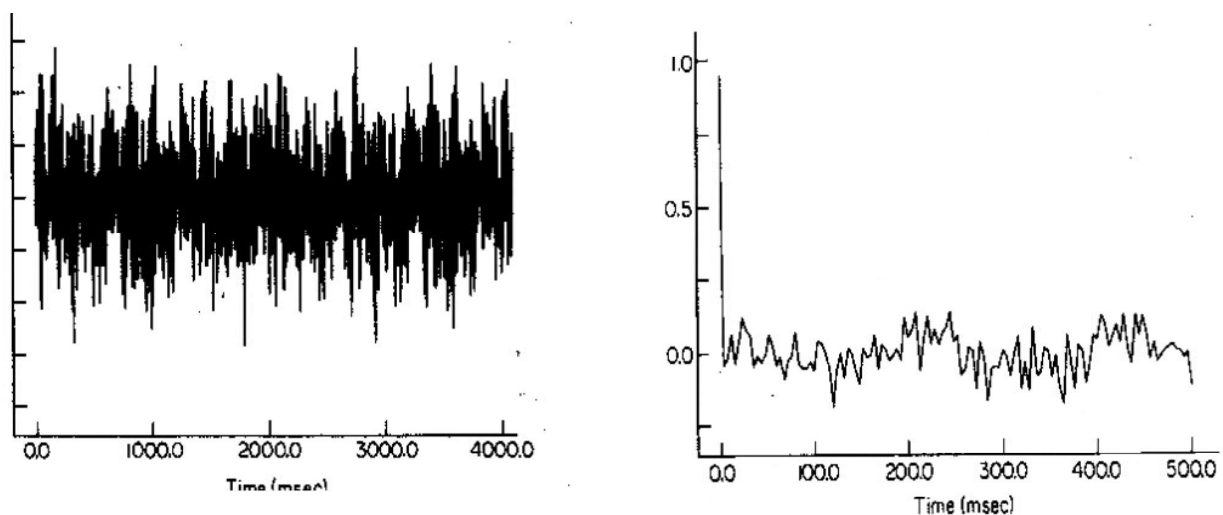


Figure 13. The auto-correlation of a random time series, after Hatton et al. (1986). Left panel, random time series; right panel, its auto-correlation.

5.2 ENHANCING MULTIPLES WITH CMP PROCESSING

Another technique for suppressing multiples is to use the different move-out characteristics of multiple and primary reflections in CMP gathers. Multiples always appear as lower velocity events than the equivalent primary. This characteristic is often employed to suppress multiples by selecting a velocity function that reinforces the primary reflection and destroys the multiples.

In this study, a water velocity function has been selected to enhance the multiples and attenuate the primary reflections below the seabed in the stacked volume. The top panel of Figure 14 shows an example CMP gather from the FINA 30/14 survey used in this study. The X-axis is the absolute offset distance and Y-axis the time. The direct arrival from the source is observed as a linear feature with an apparent velocity of 1471m/s and the primary seabed reflection appears as a hyperbolic event with an apparent velocity of 1480m/s. The lower panel of Figure 14, shows the same CMP gather after NMO with an assumed velocity of 1500m/s. For this survey a static shift of -50ms was estimated as achieving consistent velocities when examining CMP gathers. In this example the primary seabed event is slightly degraded by using a single velocity of 1500m/s, as can clearly be seen by the slight misalignment of the seabed event. This results in a smearing of the event and high frequency loss after stacking.

Having obtained a stacked volume where the multiples have been preserved and enhanced the first seabed multiple may be picked and used to map seabed topography. Furthermore, an auto-correlation volume can be created from the stacked volume and the periodicity of the seabed multiples picked, and these, too, should reflect the seabed topography.

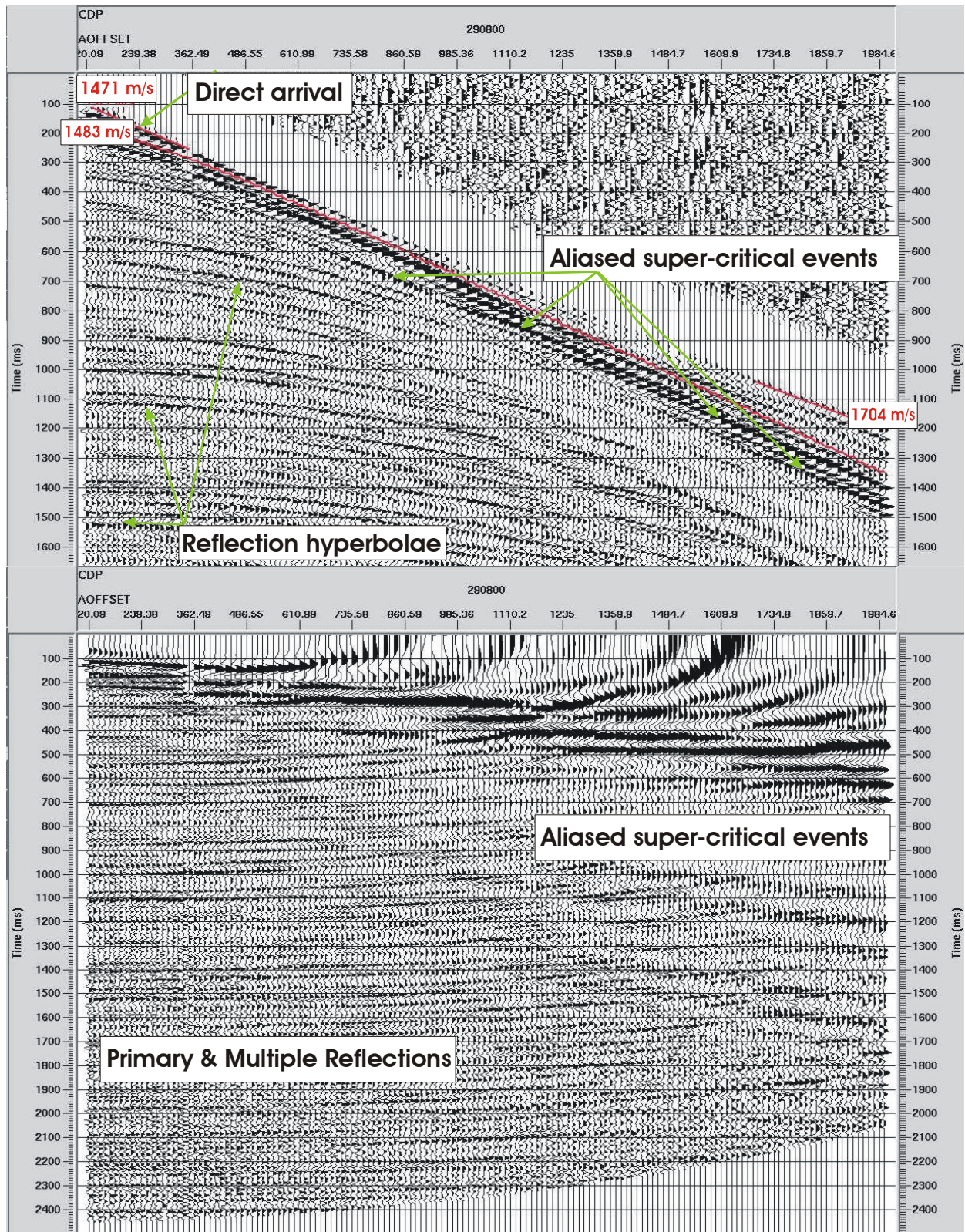


Figure 14. Example CMP displays from the FINA 30/14 survey. Top Panel; raw CMP gather, showing refraction and seabed reflection events and their apparent velocities. Bottom Panel; same CMP gather after the application of NMO with single velocity of 1500 m/s.

6 FINA 30/14 seismic survey.

The 3D survey used in this study, lies in block 30/14 of the Central Graben of the North Sea. It was originally provided to the Edinburgh Anisotropy Project (EAP) by FINA, now TOTAL for their research work. As this dataset lies in relatively shallow water, and is small in size, EAP agreed to share this dataset to permit the investigation of the approaches outlined above.

6.1 KNOWN SEABED GEOLOGY OF THE AREA COVERED BY FINA 30/14 3D SURVEY.

The survey area (Figure 15) straddles the median line between the UK and Norwegian sectors of the Central Graben of the North Sea. It lies approximately 30 km west of the Norwegian Ekofisk complex. The BGS published seabed sediments (Graham, 1986) and Quaternary geology (Fyfe, 1986) maps for the Fisher Sheet (56°N-02°E) cover the study area. The BGS maps show the area to be covered with unconsolidated sand of the Forth Formation (Early Holocene – Late Pleistocene in age) infilling a complex unconformity surface.

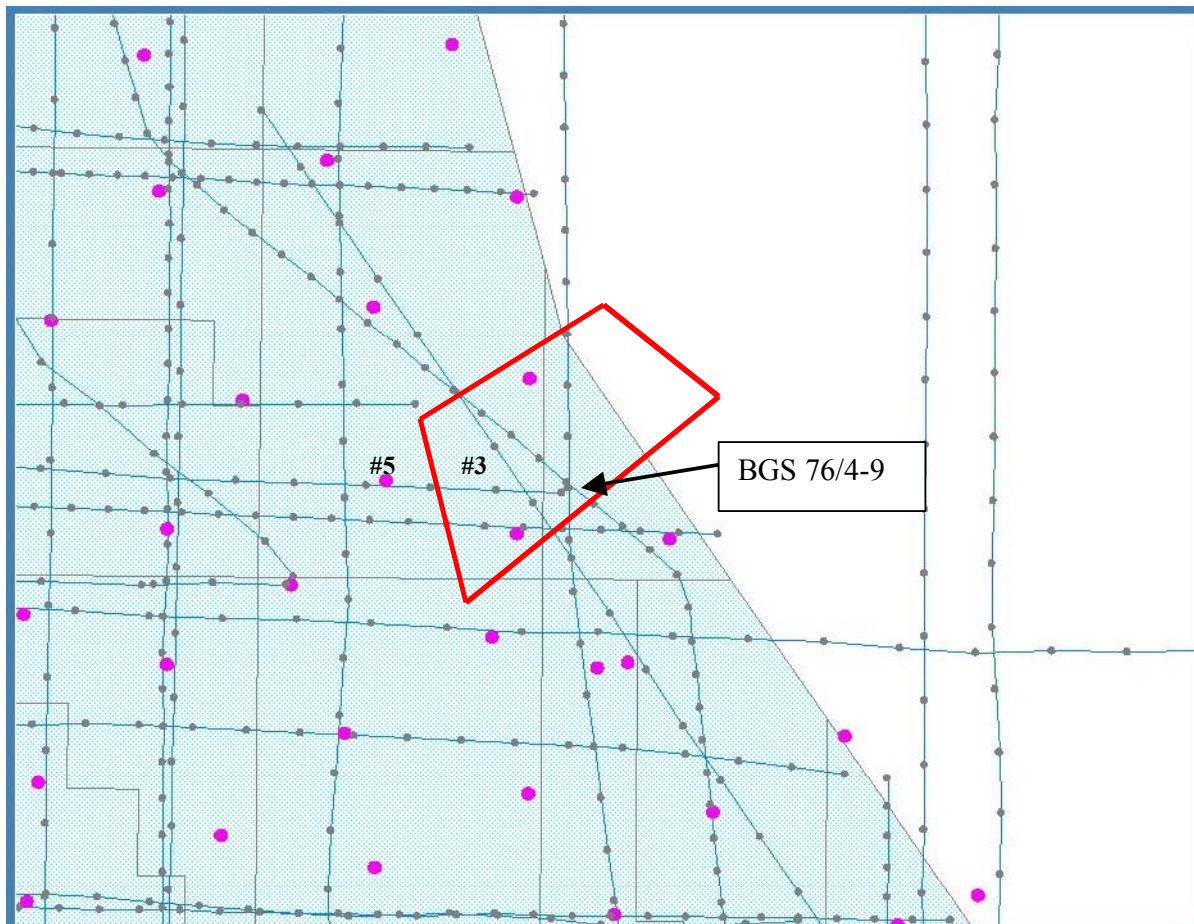


Figure 15. Study area showing BGS line tracks, BGS sample sites (pink circles) and outline of 3D seismic survey (red line) FINA 30/14 used in this study.

The unconformity cuts into the Fisher Formation (Pleistocene in age), which consists of over-consolidated clay, silt and shelly sand. Figure 17 is a bathymetry map generated from DigBath250; a BGS product of digitised bathymetric contours based on the available BGS high-resolution seismic grid displayed in Figure 15. Water depths in the immediate vicinity of the survey vary very gently around 70m. Figure 15 also shows the available BGS sample sites. Examination of echo sounder and pinger records shows very little in the way of topography at

the seabed, although the wide line spacing may be hiding small-scale bathymetric variations. However, there is evidence from BGS 76/4-9 pinger record (Figure 16) that there is significant variation in the thickness of the Forth Formation, ranging from 25ms to only a few milliseconds.

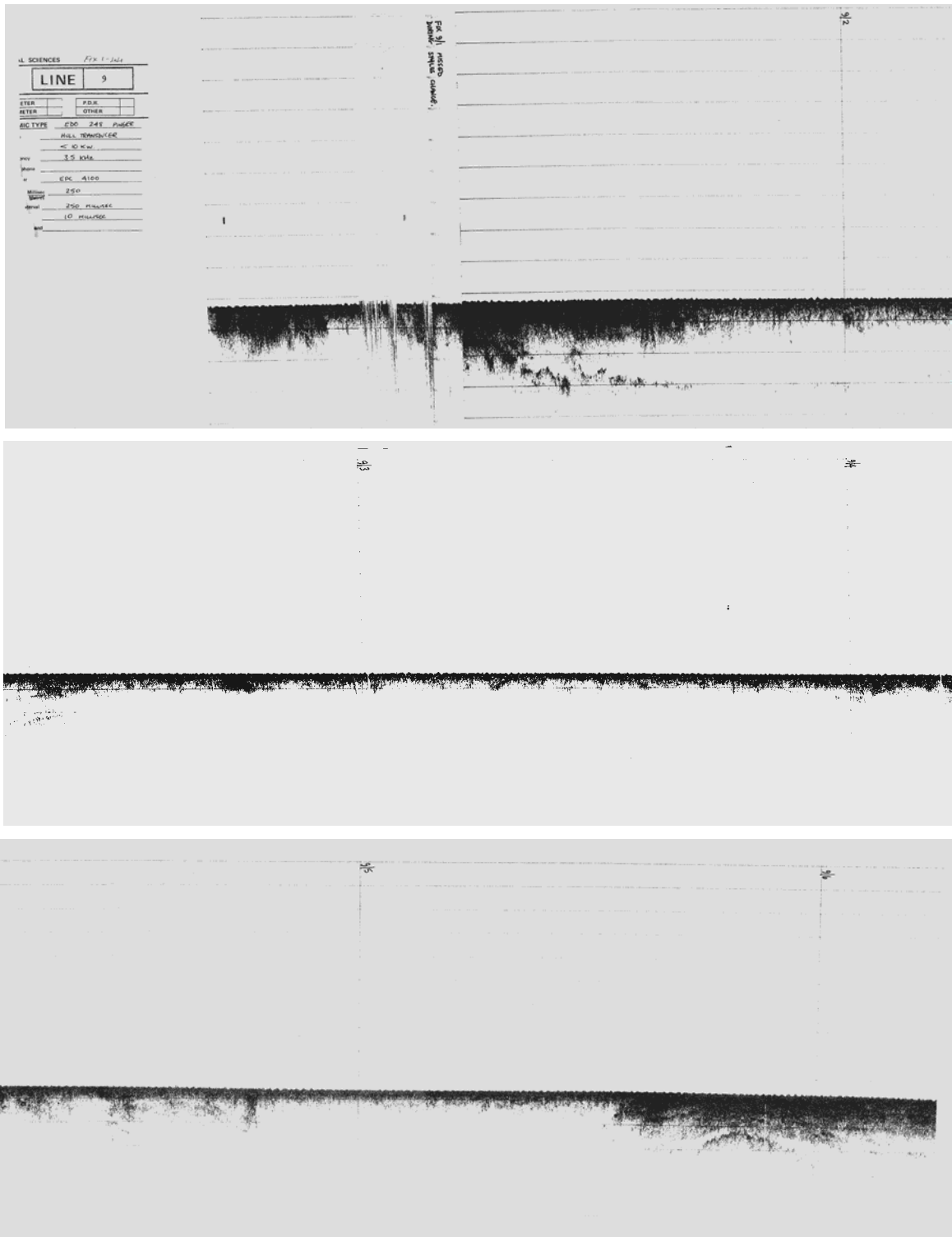


Figure 16. Pinger profile BGS 76/4-9. Fixes 2-6 showing variation in thickness of Forth Formation. Time lines 10ms.

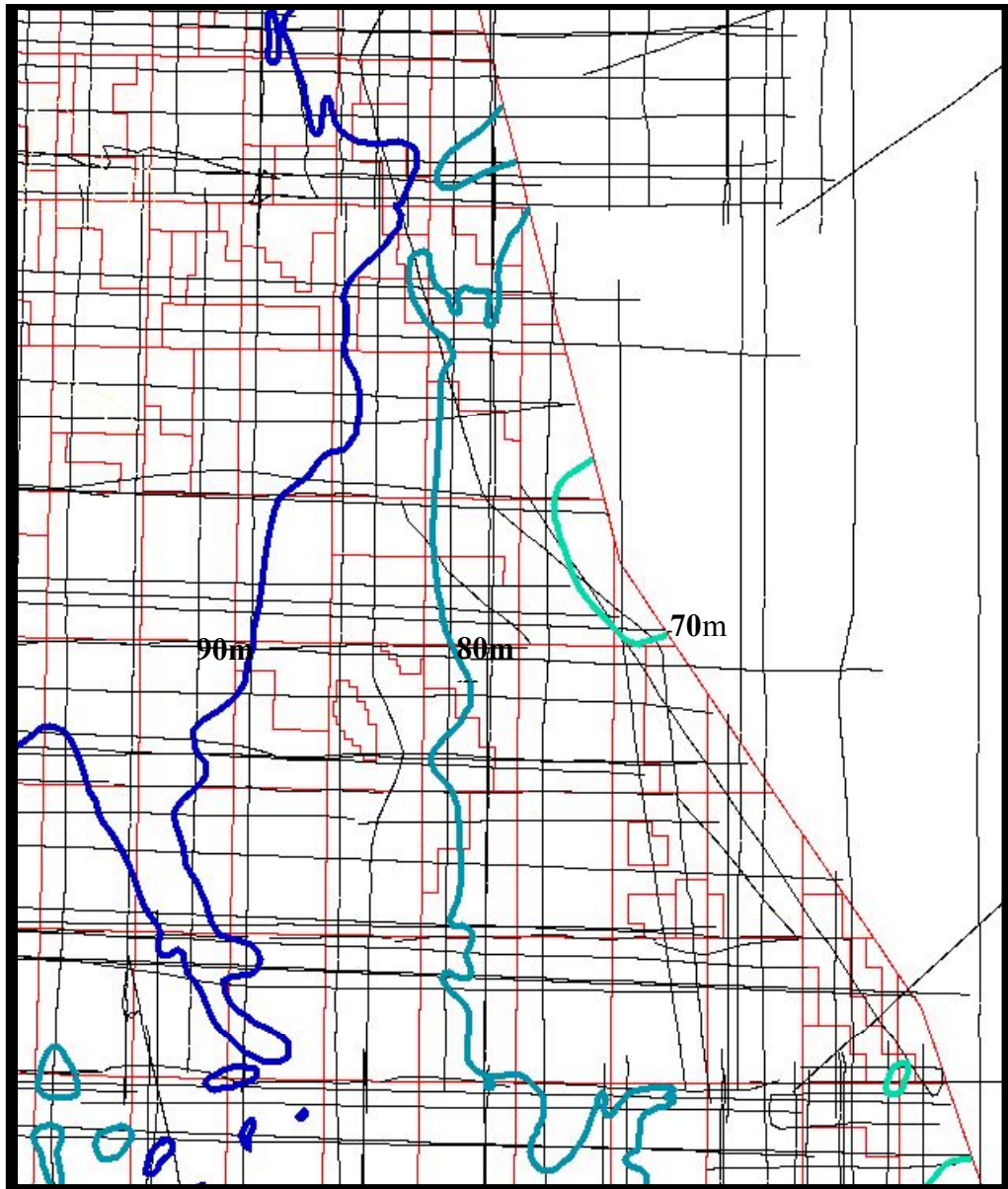


Figure 17. Regional bathymetry contours from 1:250K DigBath250 compilation. BGS profiles shown in black. UK block boundaries and median line shown in red.

footprint. At depth, close to the target depth of 3 km, the long offsets may help to in-fill the gaps. The best bin size was calculated as 50m.

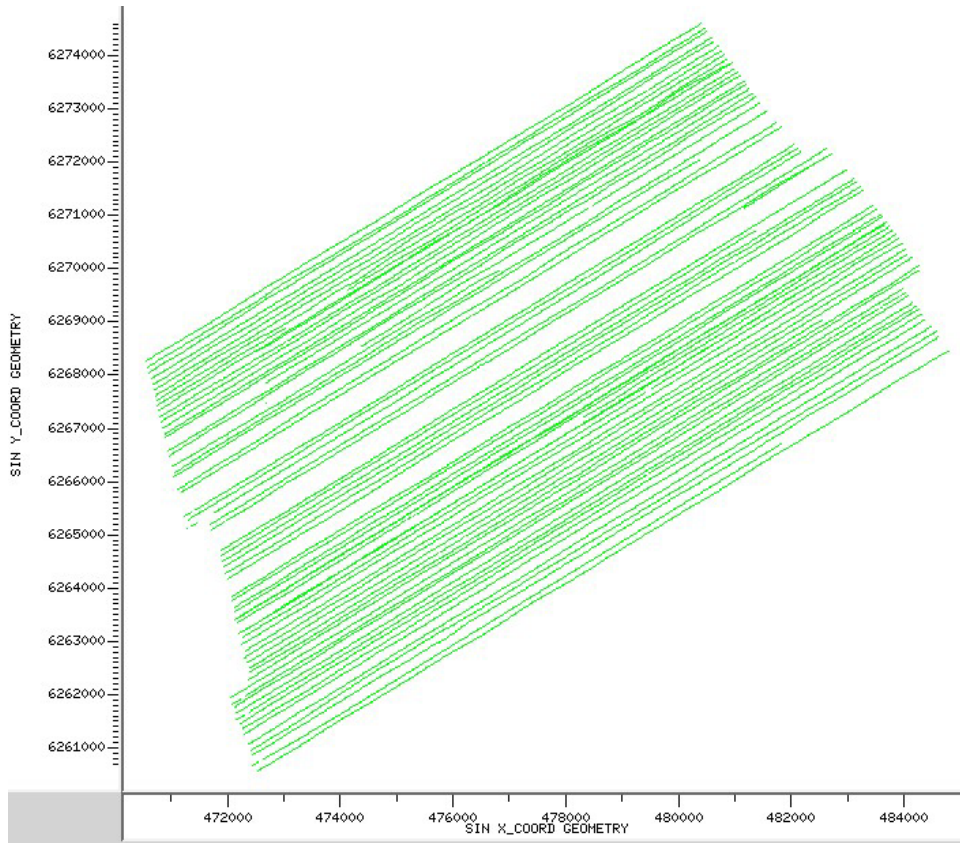


Figure 18. Shot location map

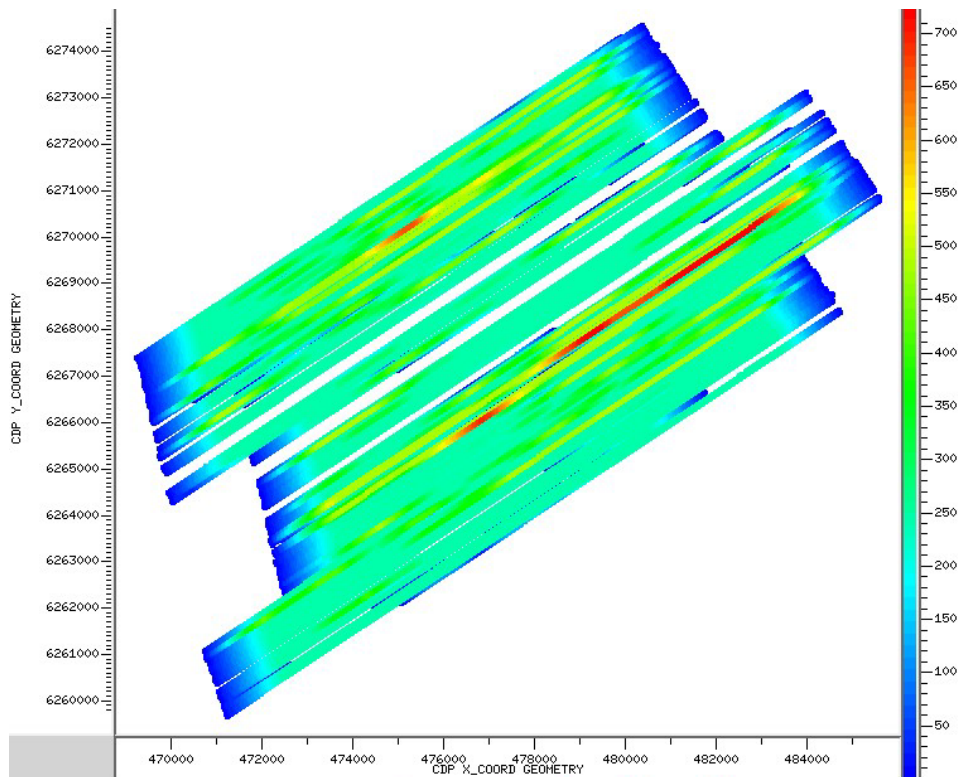


Figure 19. CMP fold coverage

7 Results of multiple stack processing

Two data volumes with bin sizes of 50m were created. The first is a near trace multiple stack volume, the second an auto-correlation volume derived from the first. Three horizons were generated from these volumes. These were the primary seabed reflection and first seabed multiples picked on the near trace section and a seabed periodicity event based on the auto-correlation volume.

7.1 NEAR TRACE SECTION

The seabed refraction, observed on the CMP gathers (Top Panel, Figure 14) suggests that the sediments at the seafloor have a velocity of 1700m/s and that the minimum offset is 120m. The graph in Figure 10 predicts that the onset of contamination by refraction and super-critical events occurs at an offset distance of 450m. This is consistent with the observed data and implies 13 traces of useful data.

A near-trace stack volume containing traces with a maximum offset of 200m was created using a constant velocity of 1500 m/s. A maximum offset of 200m was selected as this gave an optimum primary seabed reflector. Incorporating larger offset distances in the stack tends to smear the primary seabed reflection because of the misalignment problems discussed previously. No mutes were applied.

Figure 20 shows an in-line profile of the near-trace volume. Because of the favourable acquisition geometry and seabed conditions, good primary seabed and multiple events are observed. Two possible channel features are observed at the seabed between traces 370-420 and 510-590. The edges of the features are associated with small depressions in the seabed reflection.

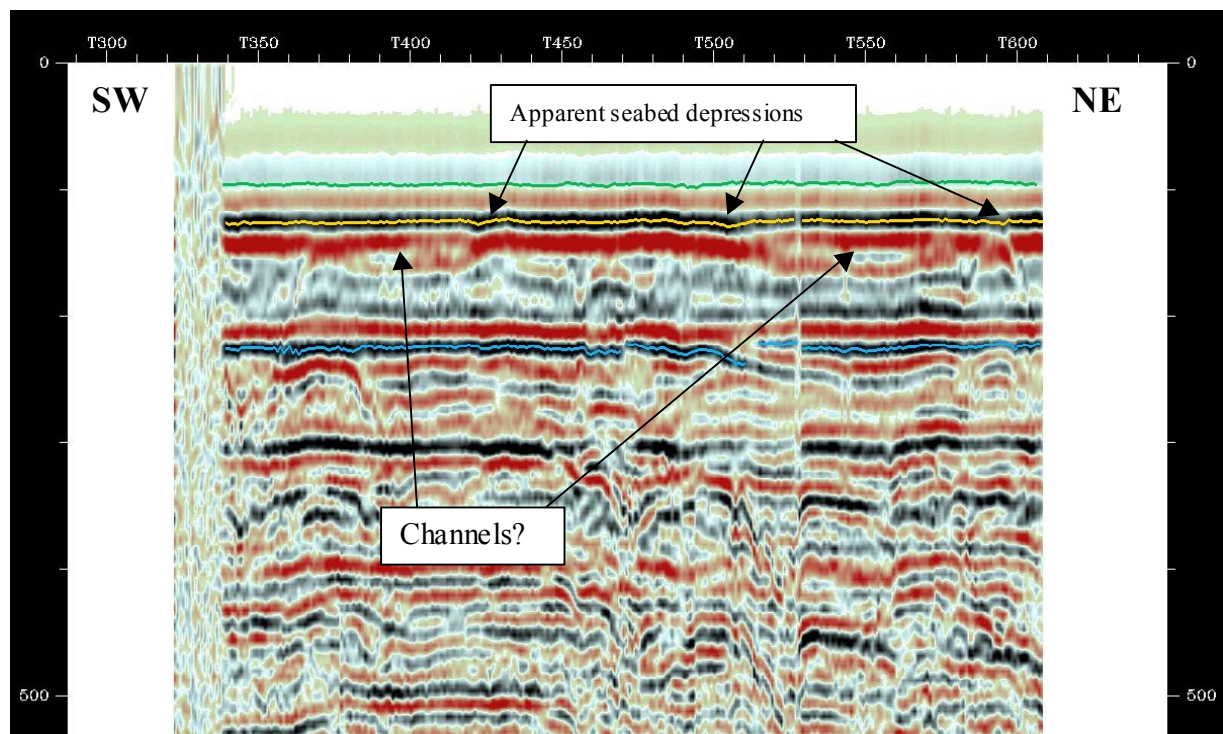


Figure 20 . Example line 397 of near-trace volume with no mutes applied. The yellow horizon is the primary seabed reflection, the cyan is the first seabed multiple and the green horizon is the seabed pick derived from an auto-correlation volume.

These may be due to the well-known thin-bed tuning effects described by Widess (1974), as the Forth formation thins abruptly, rather than true seabed topography. The first seabed multiple event also shows the features of the primary but is clearly interfered with by possible near seafloor structure at traces 460-470. The base of the right-hand channel has generated a significant multiple that has interfered with the seabed multiple, such that the auto-picking utility has partly followed the multiple of the base of the channel rather than the seabed multiple.

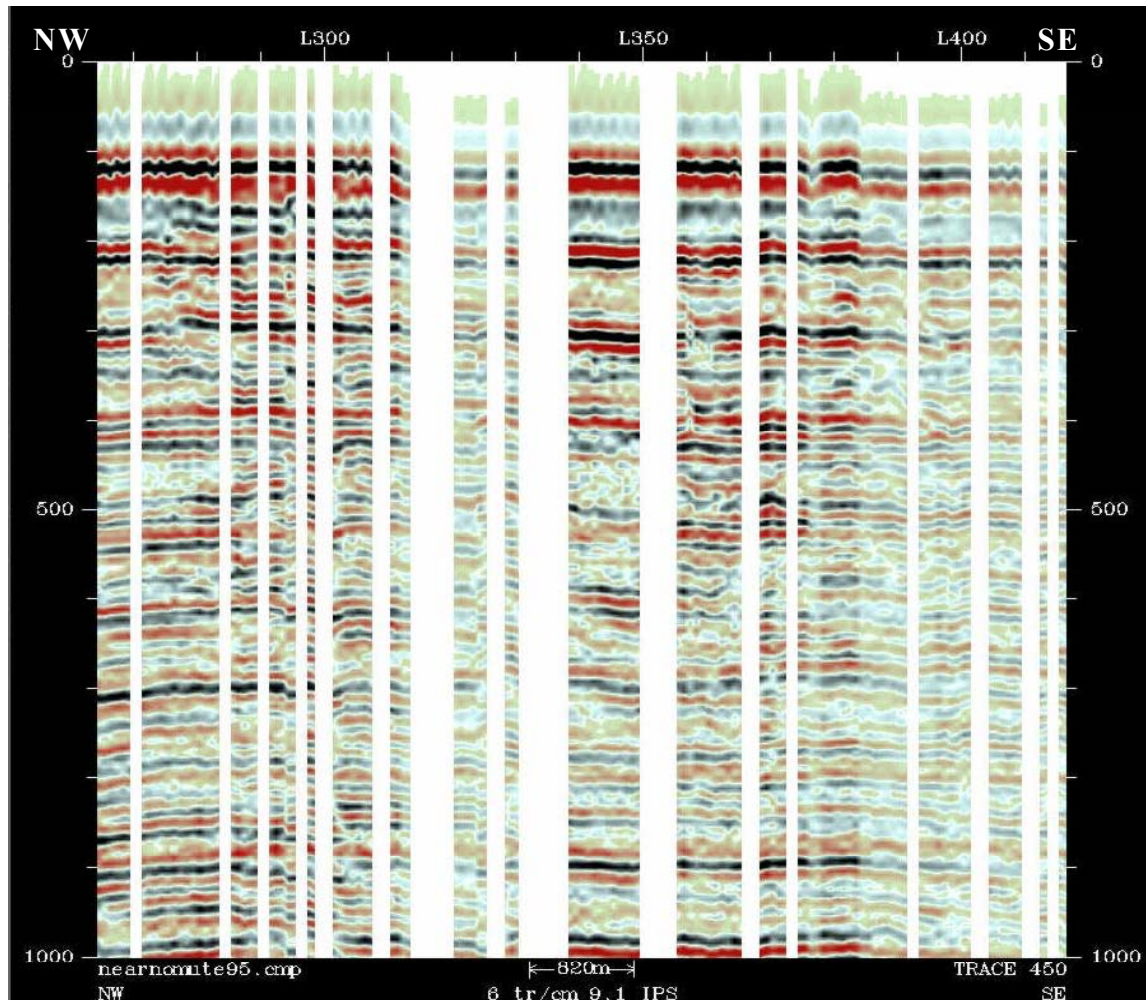


Figure 21. Example trace display (trace 452). Note the poor continuity and the abrupt changes of level of the seabed event. Note also the overall drop in amplitude between Lines 320-330 and 383-415, which are artefacts of the survey design.

Figure 21 shows a cross-line profile of the near trace volume. The profile clearly demonstrates the lack of adequate sampling in the cross-line direction, which has been commented on previously. Both the seabed and first multiple events show abrupt drops in amplitude and, as was discussed in section 4.2, has given rise to footprint anomalies that are strongest on the primary reflection and less pronounced on the first seabed multiple.

7.1.1 Primary seabed reflection map

Figures 22 and 23 are two-way time and amplitude maps respectively for the seabed reflection horizon. They are dominated by strong seismic footprint effects. Amongst the noise other features with a Northwest - Southeast orientation are discernible.

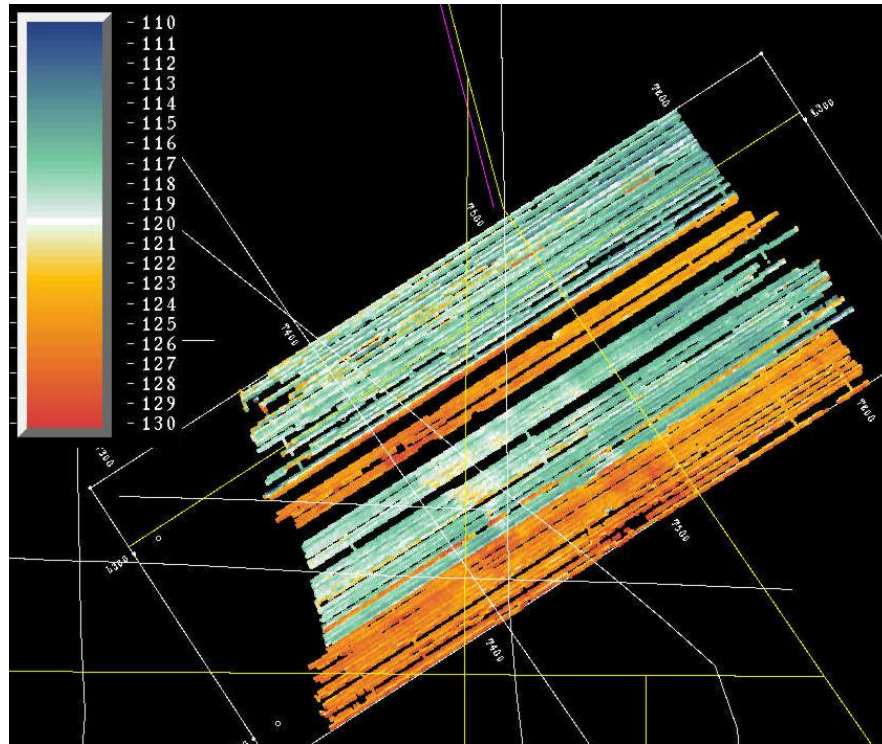


Figure 22. Map view of two-way time Zap of the seabed reflection. Note the strong impact of survey footprint artefacts and abrupt changes of levels between swaths.

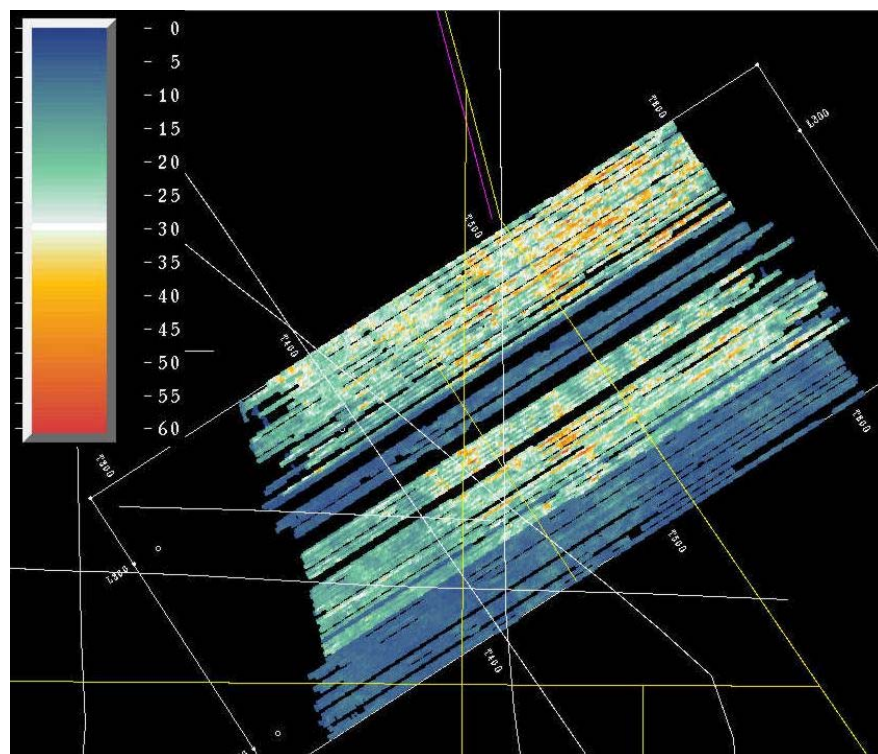


Figure 23. Map view of amplitude of seabed reflection event. Amplitudes also show strong footprint artefacts and changes between swaths.

7.1.2 First seabed multiple map

Figures 24 and 25 are two-way time and amplitude maps respectively for the first seabed multiple horizon. Seismic footprint effects are also present but less severe than for the seabed reflection horizon. As a consequence the Northwest-Southeast features observed on the seabed reflection map are clearer. However, at least part of the horizon map is contaminated with

multiple energy from the base of the channel observed on Figure 20, rather than the seabed multiple.

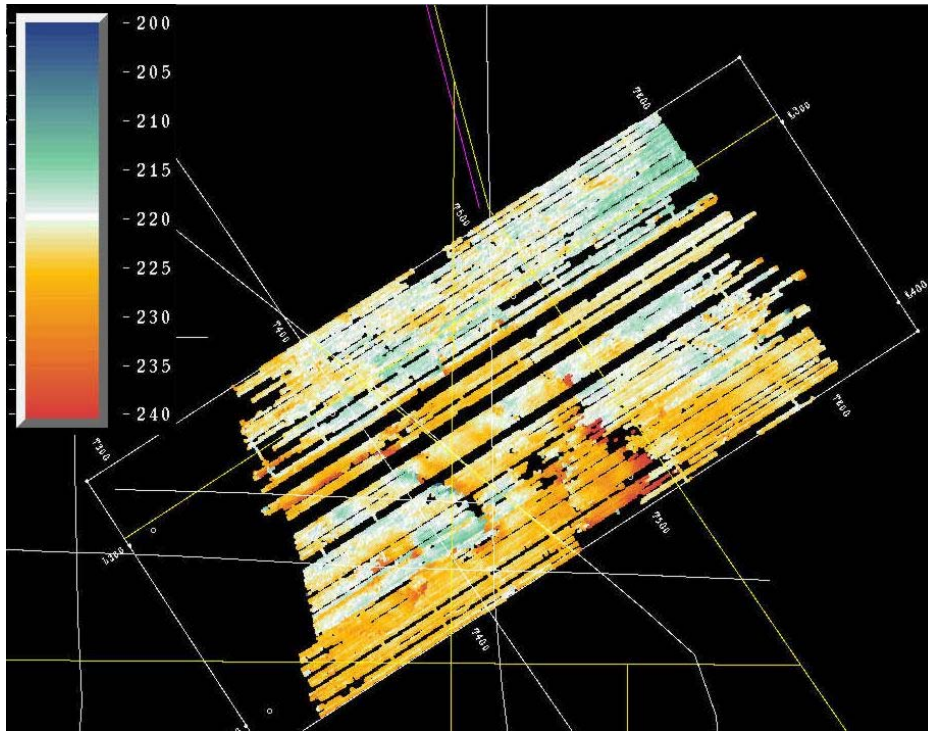


Figure 24. Map view of seabed multiple horizon. Note the reduced footprint and swath to swath shifts, so that structures are clearer. Note also the cycle skip artefacts in the south.

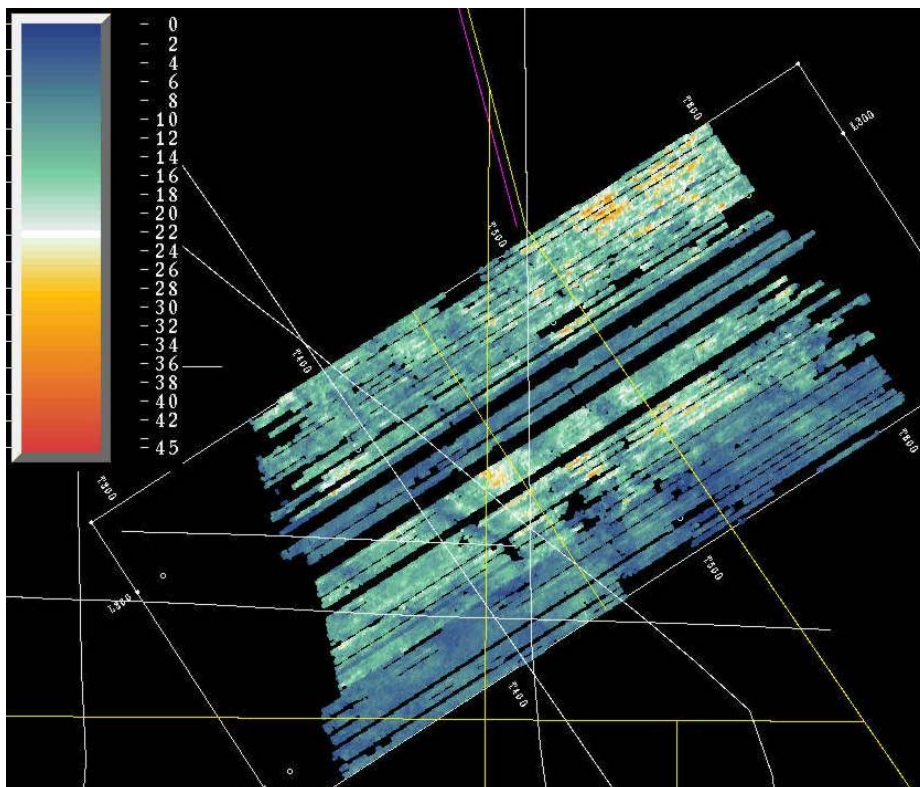


Figure 25. Amplitude map of the first seabed multiple horizon. Note the appearance of more trends in comparison to the amplitude map for the primary reflection.

7.2 SEABED PERIODICITY PICK

Figure 12 panel B shows that the auto-correlation function of a seismic trace, with a strong multiple series, is a decaying sinusoid of the period of multiple. Figure 26 shows the auto-correlation volume derived from the multiple-stack volume designed round the first multiple. A clear series of events is observed with a periodicity of about 100ms and decaying in amplitude with time. The green event represents the first lobe of this series and is an indirect estimate of the water depth. Because it measures periodicity, phase displacements due to survey footprint are removed. This is clear from Figure 27, which is the periodicity pick converted into depth using a velocity of 1480m/s. Many features are now observed and the mean depth is 70m, which coincides with the known regional bathymetry (Figure 16).

It is also of interest to consider the possible physical meaning of the amplitude of the auto-correlation function. The amplitude will reflect the strength of the correlation. As discussed in section 5.1, auto-correlation is relatively insensitive to random noise. However, if there is a larger number of multiples generated due to slightly harder seabed conditions, then one might expect stronger amplitudes in the auto-correlation. Certainly, pronounced variation in amplitude is visible in Figure 26. Figure 28 is an amplitude map of the seabed periodicity which shows features very similar in trend to those observed in the amplitude maps for the seabed reflection and its first multiple.

In comparison with the seabed reflection and first seabed multiple picks, it is clear that the seabed periodicity pick has provided the best estimate of water depth. However, it is unclear whether the map represents the true seabed topography or in fact represents thin-bed tuning effects described by Widess (1974), due to the thickness variation of the Forth formation. The lack of detailed swath bathymetry over the survey area with which to make comparison leaves this an unanswered question. However, the narrow standard deviation of the surface (mean 70.6m standard deviation 0.88m) and the association of small topographic lows with pinch-outs on profiles, makes the possibility of thin-bed tuning effects quite likely.

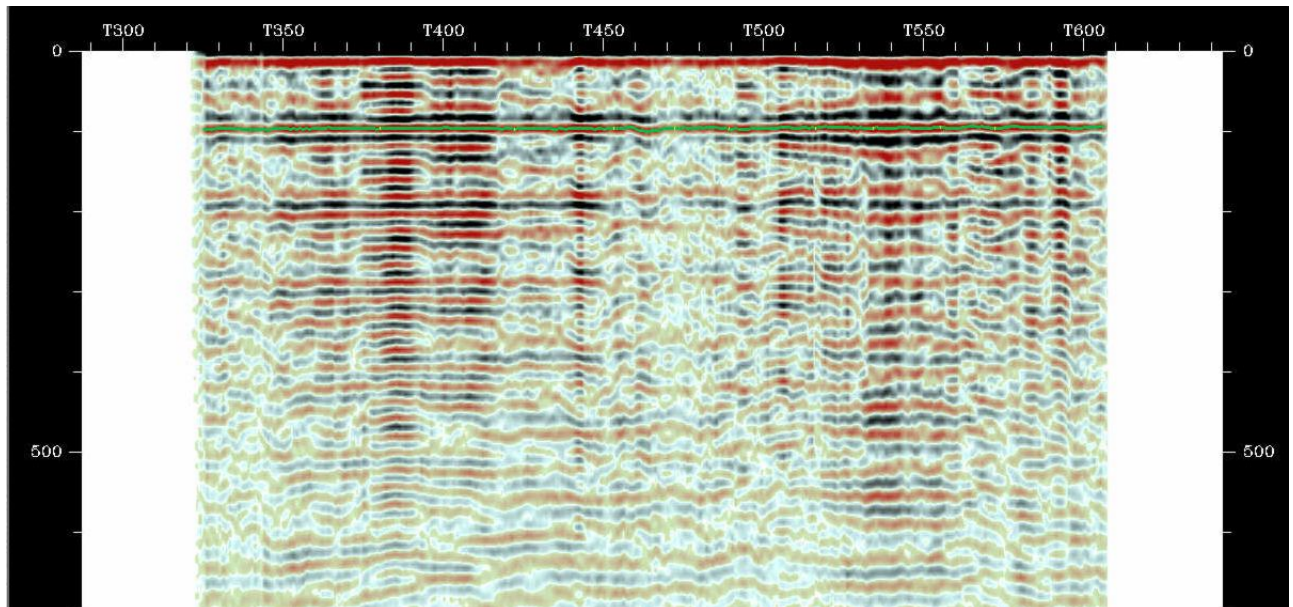


Figure 26. Example Line 387 from the auto-correlation volume designed around the first multiple

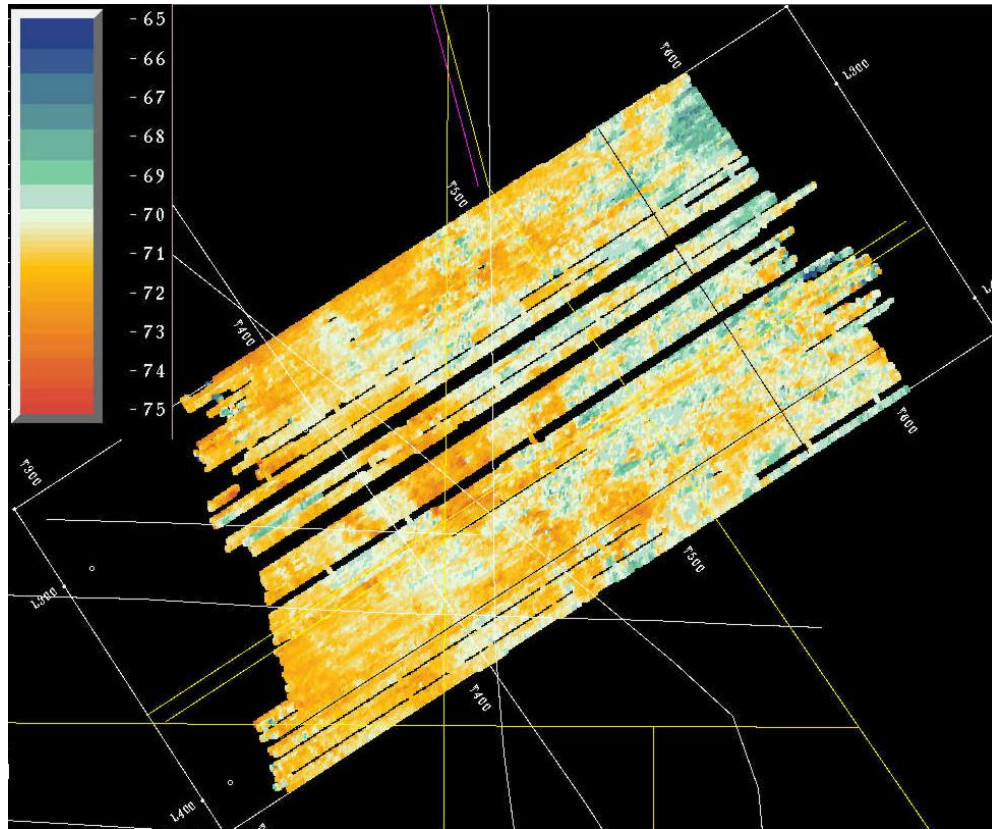


Figure 27. Water depth estimated from auto-correlation pick assuming water velocity of 1480m/s. Scale in meters.

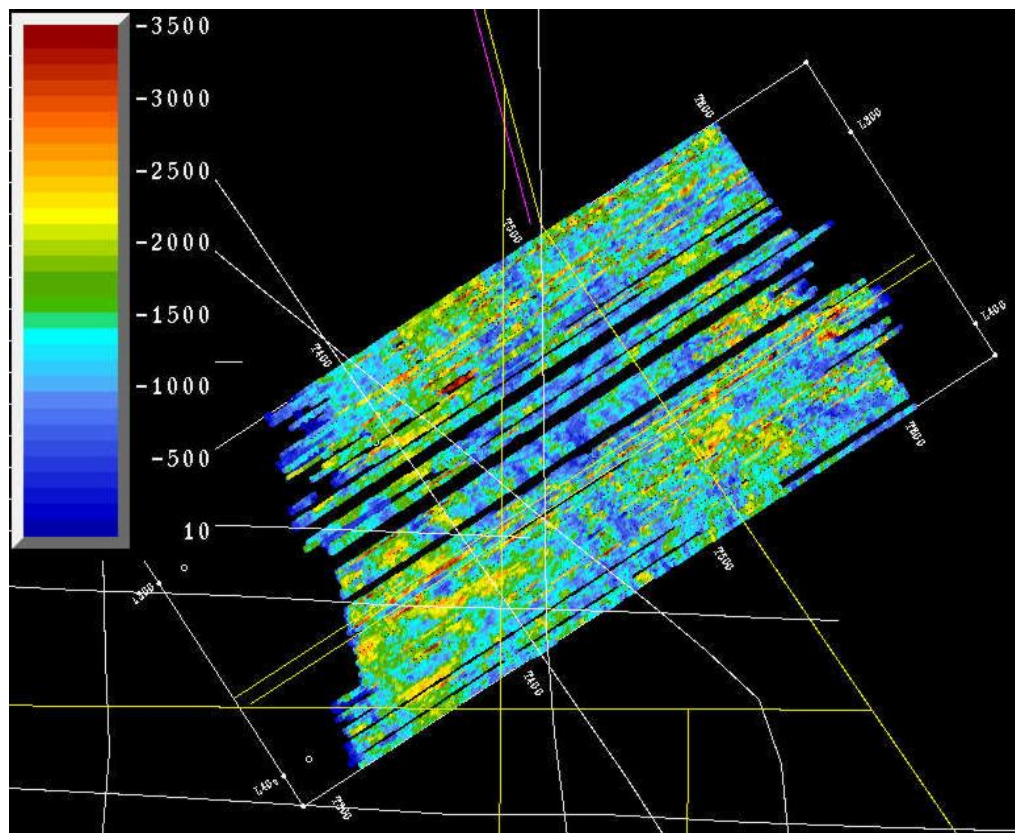


Figure 28. Amplitude map of seabed pick based on an auto-correlation volume. Scale in arbitrary units.

8 Conclusions

Seabed images based on 3D seismic produce excellent results of quality comparable to swath systems in deep water (>500m).

In shallower water depths, the survey's acquisition design and general seabed conditions become important factors in determining the image quality. Some surveys have provided excellent results in water depths of 200m, while others have been severely degraded by survey footprint artefacts at similar water depths.

As a general rule, surveys designed for imaging deep structure are less likely to generate good seabed returns, as they tend to have larger minimum offsets. Similarly, hard seabed conditions reduce the offset range over which the seabed return can be recorded, which in turn reduces the seabed image quality. Hard seabed conditions also give rise to increased levels of coherent noise generated by aliased super-critical reflectors.

Overall survey design and coverage also impact on seabed image quality, as non-uniform CMP bin populations and azimuth ranges enhance survey footprint. The survey used in this study is well sampled in the in-line direction but poorly sampled in the cross-line direction. So, although the seabed reflector is imaged, it is heavily influenced by footprint.

This study has demonstrated that the information content inherent in multiples can be used to indirectly estimate seabed topography. It requires pre-stack processing to preserve the multiple energy. For this survey, picking seabed periodicity on an auto-correlation volume has given the most convincing result. The second best result was obtained by enhancing the first seabed multiple. Seabed periodicity will become poorer in deeper water because the number of multiples present within the length of the trace record will drop and consequently the quality of the auto-correlation will degrade.

An unresolved question, due to lack of swath bathymetry in the survey region, is the extent to which the topography generated by the seabed periodicity reflects tuning effects due to the rapidly varying thickness of the Forth Formation, as opposed to the true seabed topography.

The technique needs to be applied to another, deeper water area, such as Shell's woc96 survey in the FSC where the primary seabed reflection begins to fade. This would enable a direct comparison of surfaces generated by conventional and multiple enhancement processing as well as present an opportunity to extend the FSC seabed image.

9 Acknowledgements

Thanks are due to FINA, now TOTAL, for contributing the dataset used in this study and for permission to show the data. The data was originally provided to the Edinburgh Anisotropy Project (EAP). Thanks are due to Xiang-Yang Li, head of the EAP for agreeing to share the data with the author of this report. Further thanks are due to the Western Frontiers Association for providing the 3D seismic data volumes used in the seabed image of the FSC and especially to BP for providing the detailed swath bathymetry data in the FSC study area.

10 References

Most of the references listed below are held in the Library of the British Geological Survey at Keyworth, Nottingham. Copies of the references may be purchased from the Library subject to the current copyright legislation.

- BULAT, J. & LONG, D., 2001. Images of the seabed in the Faroe-Shetland Channel from commercial 3D seismic data. *Marine Geophysical Researches*, 22, 345-367
- BULAT, J., 2003. A study of reflection amplitudes of the seabed in the Faroe-Shetland Channel derived from commercial 3D seismic surveys. British Geological Survey confidential report CR/03/127.
- CANNING, A & GARDNER, G.H.F., 1998. Reducing 3-D acquisition footprint for 3-D DMO and 3-D prestack migration. *Geophysics*, 63, 1177-1183.
- CONEY, D., FYFE, T.B., RETAIL, P. AND SMITH, P.J., 1993. Clair appraisal: the benefits of a co-operative approach. In: Parker, J.R. (ed.) *Petroleum Geology of Northwest Europe: Proceedings of the 4th Conference*. Geological Society, London, pp.1409-20.
- DRUMMOND, D., BUDD, A.J.L. AND RYAN, J.W., 2000. Adapting to noisy 3D data – attenuating the acquisition footprint. Extended abstracts Soc. Explor. Geophys. Annual meeting, Calgary 2000.
- FYFE, J. A., 1986. FISHER (56°N-02°E), 1:250,000 Quaternary Geology Map Sheet. British Geological Survey.
- GRAHAM, C., 1986. FISHER (56°N-02°E), 1:250,000 Seabed Sediments Map Sheet. British Geological Survey.
- HATTON, L., WORTHINGTON, M.H. AND MAKIN, J., 1986. *Seismic Data Processing*, Blackwell Scientific Publications.
- HILL, S., SCHULTZ, M. & BREWER, J., 1999. Acquisition footprint and fold-of-stack plots. *The Leading Edge*, June 1999, 686-695.
- HOLMES, R., BULAT, J., HAMILTON, I., & LONG, D., 2003. Morphology of an ice-sheet limit and constructional glacially-fed slope front. Faroe-Shetland Channel. In: *European margin sediment dynamics: side-scan sonar and seismic images* (Eds. J. Mienert, P. Weaver) Springer-Verlag, Berlin Heidelberg.
- LANSLEY, W., 1996. Considerations for optimum 3-D survey design, acquisition and processing. In: *The interpretation of three-dimensional seismic data*. Fourth Edition, (Brown, A. R.) AAPG Memoir 42. AAPG, Appendix A, pp 397-402.
- LONG, D. BULAT, J. & STOKER, M.S., in press. Sea bed morphology of the Faroe-Shetland Channel derived from 3D seismic data sets. In: *3D Seismic Data: application to the exploration of sedimentary basins*. (Eds. Davies, R., Cartwright, J., Stewart, S., Underhill, J., and Lappin, M.) Geological Society of London Memoir.
- MARFURT, K.J., SCHEET, R.M., SHARP, J.A AND HARPER, M.G., 1998. Suppression of the acquisition footprint for seismic sequence attribute mapping. *Geophysics*, 62, 1774-1778.
- PAUL, M.A., TALBOT, L.A. & STOKER, M.S., 1993. Geotechnical properties of sediments from the continental slope northwest of the British Isles. Volume 28: *Offshore Site Investigation and Foundation Behaviour*, Soc. for Underwater Technology, 77-106.
- STOKER, M.S., 1999. Stratigraphic nomenclature of the UK North West Margin. 3. Mid- to late Cenozoic stratigraphy. British Geological Survey. Edinburgh.
- WIDESS, M. B., 1973, How thin is a thin bed? *Geophysics*, 38, 1176-1180.
- YILMAZ, O., 2001. Seismic data analysis, processing, inversion and interpretation of seismic data. *Investigations in geophysics series no. 10* (Ed by Doherty, S. M.), Soc. Explor. Geophys. Tulsa.